4

OFFICE OF NAVAL RESEARCH

Contract N00014-82-K-0576

Technical Report No. 41

ADSORPTION OF ORGANO-RHODIUM SPECIES ON METAL-OXIDE SURFACES: THEORETICAL ASPECTS

by

J.-F. Halet and R. Hoffmann

Department of Chemistry
Cornell University
Baker Laboratory
Ithaca, NY 14853-1301

July 1988

Reproduction in whole or in part is permitted
for any purpose of the United States Government

This document has been approved for public release
and sale; its distribution is unlimited

SECURITY CLASSIFICATION OF THIS PAGE

REPORT DOCUMENTATION PAGE

1a. REPORT SECURITY CLASSIFICATION

1b. RESTRICTIVE MARKINGS

2a. SECURITY CLASSIFICATION AUTHORITY

3. DISTRIBUTION/AVAILABILITY OF REPORT

2b. DECLASSIFICATION/DOWNGRADING SCHEDULE

4. PERFORMING ORGANIZATION REPORT NUMBER(S)
#41

5. MONITORING ORGANIZATION REPORT NUMBER(S)

6a. NAME OF PERFORMING ORGANIZATION
Department of Chemistry

6b. OFFICE SYMBOL *(If applicable)*

7a. NAME OF MONITORING ORGANIZATION
ONR

6c. ADDRESS *(City, State, and ZIP Code)*
Cornell University
Baker Laboratory
Ithaca, NY 14853-1301

7b. ADDRESS *(City, State, and ZIP Code)*
800 Quincy St., Arlington

8a. NAME OF FUNDING/SPONSORING ORGANIZATION

8b. OFFICE SYMBOL *(If applicable)*

9. PROCUREMENT INSTRUMENT IDENTIFICATION NUMBER
Report #41

8c. ADDRESS *(City, State, and ZIP Code)*

10. SOURCE OF FUNDING NUMBERS

PROGRAM ELEMENT NO.	PROJECT NO.	TASK NO.	WORK UNIT ACCESSION NO

11. TITLE *(Include Security Classification)*
Adsorption of Organo-Rhodium Species on Metal-Oxide Surfaces: Theoretical Aspects

12. PERSONAL AUTHOR(S)
J.-F. Halet and R. Hoffmann

13a. TYPE OF REPORT
Technical Report #41

13b. TIME COVERED
FROM ________ TO ________

14. DATE OF REPORT *(Year, Month, Day)*
July 20, 1988

15. PAGE COUNT

16. SUPPLEMENTARY NOTATION

17. COSATI CODES

FIELD	GROUP	SUB-GROUP

18. SUBJECT TERMS *(Continue on reverse if necessary and identify by block number)*

19. ABSTRACT *(Continue on reverse if necessary and identify by block number)*

Tris(allyl)rhodium reacts with hydroxylated TiO_2 and Al_2O_3 surfaces to produce oxide-bound bis(allyl)rhodium which, upon addition of H_2, forms oxide-bound (allyl)rhodiu hydride species. The nature of the rhodium-oxygen bonding and the role of the inorganic support are analyzed via extended Hückel band calculations on two-dimensional slabs of metal oxide and organo-rhodium adsorbates. Side by side with this analysis we looked at discrete molecular analogues of the surface species. One-, two-oxygen-bound Rh(allyl) and one-, two- and three-oxygen-bound Rh(allyl)(H) models were examined. There are great similarities between the isolated molecule models and the supported interactions. Crucial to the role of the oxide support is its partial reduction, through defect structures, and resonances between support and adsorbate energy levels. The oxide suppor not only serves to immobilize the organometallic adsorbate, but might also act as an electron reservoir or electron sink, depending upon the electronic requirements of the adsorbed complexes.

20. DISTRIBUTION/AVAILABILITY OF ABSTRACT
☒ UNCLASSIFIED/UNLIMITED ☐ SAME AS RPT. ☐ DTIC USERS

21. ABSTRACT SECURITY CLASSIFICATION

22a. NAME OF RESPONSIBLE INDIVIDUAL
Roald Hoffmann

22b. TELEPHONE *(Include Area Code)*
607-255-3419

22c. OFFICE SYMBOL

DD FORM 1473, 84 MAR

83 APR edition may be used until exhausted
All other editions are obsolete.

SECURITY CLASSIFICATION OF THIS PAGE

ADSORPTION OF ORGANO-RHODIUM SPECIES ON METAL-OXIDE SURFACES: THEORETICAL ASPECTS

Jean-François Halet[§] and Roald Hoffmann*
Department of Chemistry and Materials Science Center
Baker Laboratory, Cornell University, Ithaca, NY 14853-1301

Abstract: Tris(allyl)rhodium reacts with hydroxylated TiO_2 and Al_2O_3 surfaces to produce oxide-bound bis(allyl)rhodium which, upon addition of H_2, forms oxide-bound(allyl)rhodium hydride species. The nature of the rhodium-oxygen bonding and the role of the inorganic support are analyzed via extended Hückel band calculations on two-dimensional slabs of metal oxide and organo-rhodium adsorbates. Side by side with this analysis we looked at discrete molecular analogues of the surface species. One-, two-oxygen-bound $Rh(allyl)_2$ and one-, two- and three-oxygen-bound Rh(allyl)(H) models were examined. There are great similarities between the isolated molecule models and the supported interactions. Crucial to the role of the oxide support is its partial reduction, through defect structures, and resonances between support and adsorbate energy levels. The oxide support not only serves to immobilize the organometallic adsorbate, but might also act as an electron reservoir or electron sink, depending upon the electronic requirements of the adsorbed complexes.

[§] Permanent address: Laboratoire de Cristallochimie, UA 254, Université de Rennes I, 35042 Rennes France

The chemistry of oxide-bound organometallic species constitutes a new and important area of the heterogeneous catalysis.[1] Most of the studies have been done on polycrystalline or powder samples. Understanding of the adsorption mechanism on an atomic scale requires the characterization of both the adsorbed molecule and the metal oxide surface, i.e. the composition, the atomic positions and the eventual rearrangements of the studied system. Theoretical studies can aid in obtaining a picture of the mechanism.

Recently, Bernasek, Schwartz and colleagues[2] have reported that tris(allyl)rhodium reacts on hydroxylated metallic oxide surfaces (titania and alumina) to produce a bis(allyl)rhodium surface species. Upon subsequent reaction with hydrogen, an (allyl)rhodium hydride complex is formed. This hydride species, when anchored on the oxide surface, exhibits unusual catalytic activity for hydrogenation of alkenes and arenes (Scheme 1).

Scheme 1 here

The originality of the Princeton work derives from the way it was carried out, on single-crystal surfaces under ultra-high vacuum conditions, allowing access to information at a molecular level through UPS, ELS and AES measurements. Although precursor and catalytic derivatives attached to oxide supports are rather well-characterized, the nature of the rhodium-oxygen bonding (i.e., strong or weak, homopolar or ionic) and the influence of the inorganic support on the acid/base properties of the active

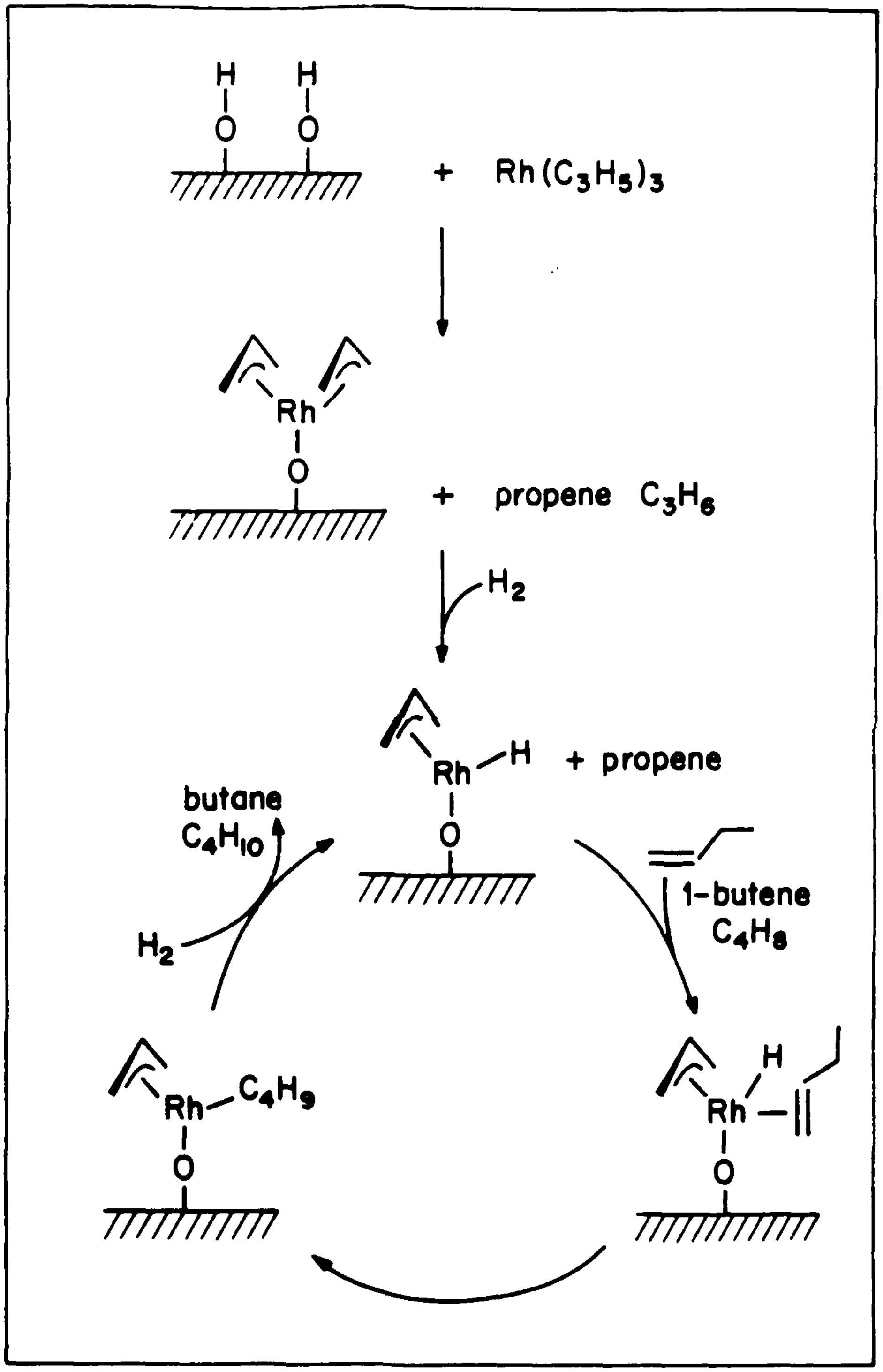
H
O
H
O
+ $Rh(C_3H_5)_3$
Rh
O
+ propene C_3H_6
H_2
Rh
H
+ propene
O
butane
C_4H_{10}
H_2
1-butene
C_4H_8
Rh
C_4H_9
O
H
Rh
O

Scheme 1

sites are really not understood. For instance, we do not know if more than one oxygen atom interacts with the rhodium center during the reaction. The purpose of this report is to analyze and discuss the electronic consequences of the chemisorption of the bis(allyl)rhodium and the (allyl)rhodium hydride species on a hydroxylated metallic oxide surface, namely the rutile TiO_2 (011) surface. This is done by using tight-binding calculations of the extended Hückel type.

The natural way to construct the system theoretically is by assemblage of the organo-rhodium fragments (adsorbates) with the inorganic counterpart (adsorbent). We arbitrarily chose to consider the active site of the hydroxylated substrate, the oxygen atom, as an anionic species. Thus, we shall approach the cation complex $[Rh(C_3H_5)_2]^+$ (14 electrons) and $[Rh(C_3H_5)(H)]^+$ (12 electrons) to one or more oxygen atoms of the metal oxide surface TiO_2 (011).

There are two popular ways to think about heterogeneous catalytic phenomena. One is a collective approach, which originates from the band theory of the electronic structure of solids.[3] The surface is considered as an infinite periodic crystal lattice, where electrons can be transferred over large distances. The chemisorption of adsorbed species is then treated by taking into account the symmetry of the regular crystal lattice and ability of electrons to be localized within the adsorption region. The other approach is a local one, one which considers the interactions of adsorbed molecules only with the nearest atoms of the surface, i.e. a molecular model approach.[4]

The two approaches are not mutually exclusive.[5] They should converge. So we shall use the two methods, local and collective, to analyze the nature of the bonding between the metal center of the adsorbate and the anchoring oxygen sites of the adsorbent. The analysis of interactions in the solid is made easier by prior knowledge of the related interactions taking place in discrete models. Also we intend eventually to compare the bonding between rhodium and oxygen atoms in discrete molecules and metal oxide surfaces.

Oxygen-rhodium bonding in discrete molecules

The ubiquitous η^3-allyl ligand, occupying two-coordination sites, forms moderately stable complexes with virtually all the transition metal series. Originally anchored to a metal center, it can be relatively easily displaced by incoming substrates. This property allows these compounds to be excellent precursors for the preparation of homogeneous or heterogeneous catalysts. In the present case, as noted above, one allyl ligand of tris(allyl)rhodium complex is presumably displaced as propene and the resulting bis(allyl)rhodium cationic species is immobilized on the metal oxide surface through rhodium-oxygen bonds. Is the rhodium atom coordinated to one or more oxygen sites? In other words, is the oxide-bound bis(allyl)rhodium characterized by 16 or 18 electrons?

Before trying to answer this question, let us review the chemistry of bis(allyl) transition metal molecules. It resembles, to some extent, the chemistry of bis(cyclopentadienyl) complexes MCp_2. Indeed, in both cases, the compounds do not rigidly conform to the 18-electron rule. Moreover, they can be highly symmetric, with parallel carbon ligands, or they can bend and add some extra ligands in order to achieve their electronic requirements. Bis(allyl)nickel is a 16-electron species.[6] Bis(allyl)nickel trimethylphosphine[7] or tris(allyl)rhodium[8] possess 18 electrons. An 18-electron count is generally preferred with σ-donor ligands for bis(allyl)ML_n complexes. What about bis(allyl)ML_n species with π-donor oxo-ligands? Such complexes seem rather scarce. To our knowledge, only two rhodium compounds have been structurally characterized[9-10], 1 and 2.

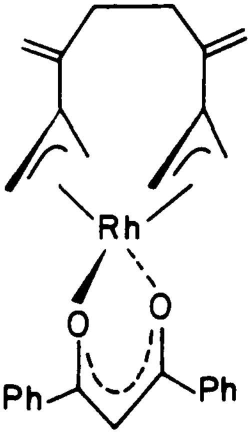

1

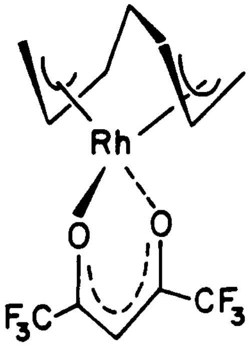

2

Both of these organo-rhodium(III) species are 18-electron complexes. Assuming that the η^3-allyl ligand occupies two coordination sites, compounds 1 and 2 describe approximately a "trigonal prismatic" structure 3.

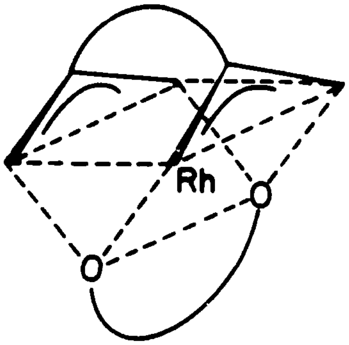

3

The "trigonal prismatic" model, $[Rh(C_3H_5)_2(OH)_2]^-$

Let us analyze the nature of bonding between the rhodium center and the oxo-ligands on the molecular model $[Rh(C_3H_5)_2(OH)_2]^-$, 4 (see the Appendix for the geometrical details). The system can be built from the interaction of the bis(allyl)rhodium cation with the $[(OH)_2]^{2-}$ group, which mimics the acetylacetonate ligand present in 1 or 2. The frontier orbitals of the $[Rh(C_3H_5)_2]^+$ fragment, shown on the left in Figure 1, are easily understood if we consider such a fragment analogous to an ML_4 C_{4v} square pyramidal structure obtained upon distortion of an ML_4 D_{4h} square planar pyramid.[11]

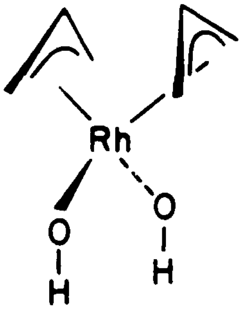

4

Figure 1 here

Indeed the MO's boxed by a dashed line in Figure 1 match rather well the orbitals of the ML_4 square pyramidal fragment of C_{4v} symmetry shown in 5. In brackets are the labels of the orbitals in C_{2v} symmetry, which is the actual symmetry of the

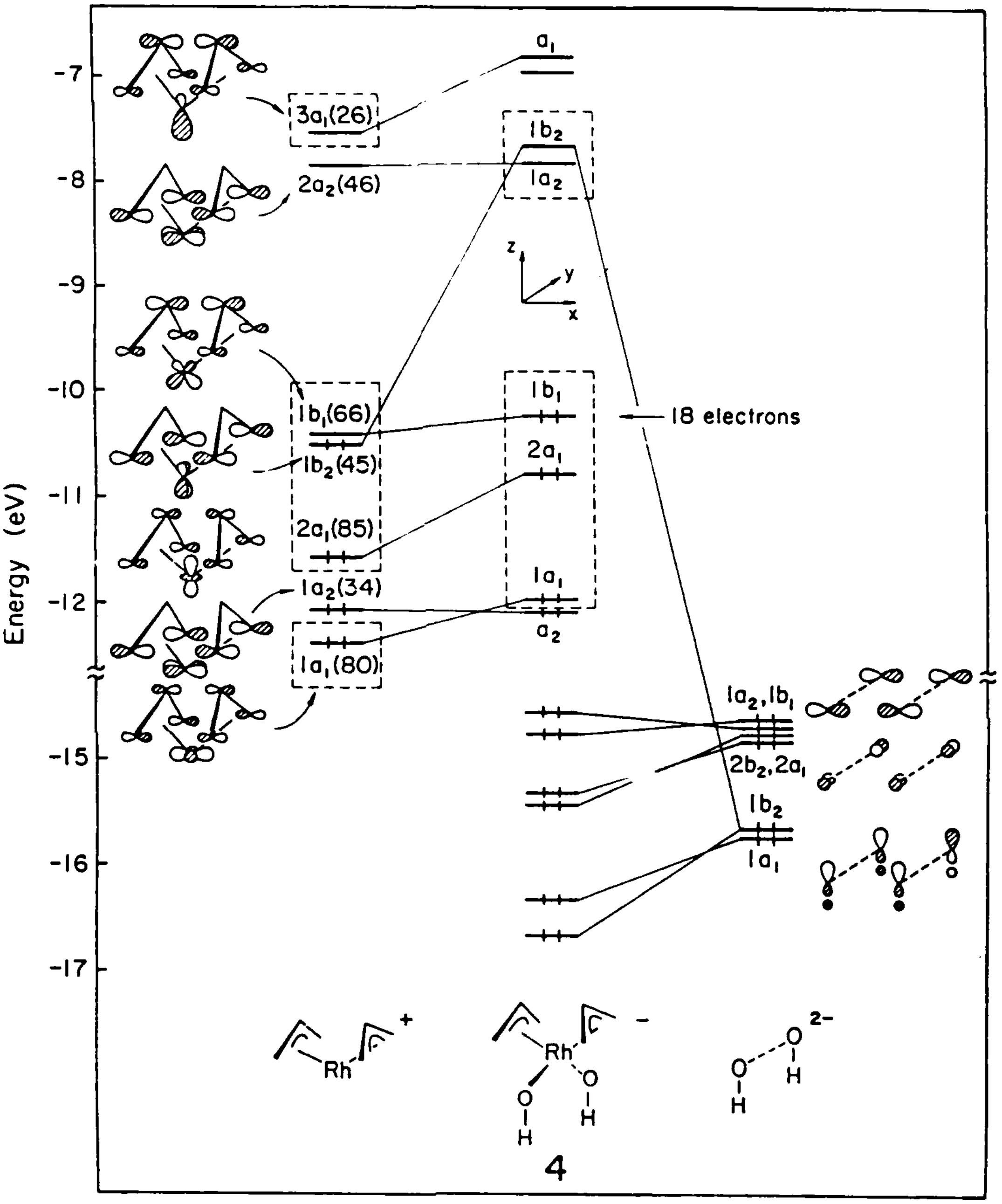

Figure 1. Interaction diagram for $[Rh(allyl)_2(OH_2]^-$ (the numbers in parentheses indicate the percentage metal character).

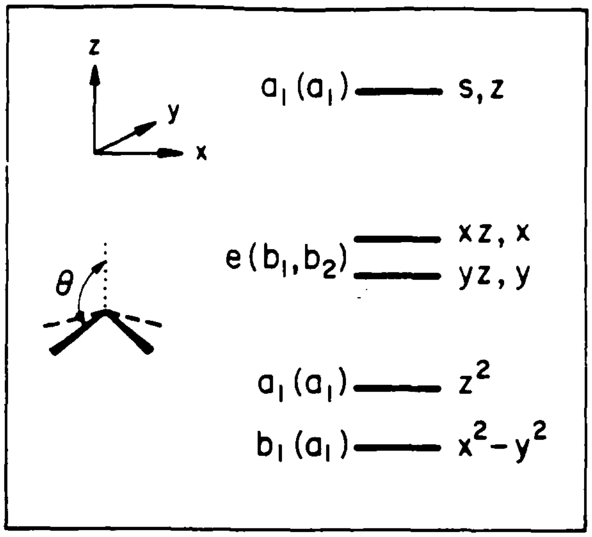

5

bis(allyl)rhodium moiety. With a 14-electron fragment, the orbitals $1a_1$, $2a_1$ and $1b_2$ are occupied, and the two others, $1b_1$ and $3a_1$ are vacant. Among these, the three upper fragment molecular orbitals (FMO's) $1b_2$, $1b_1$ and $3a_1$ are expected to play a major role in interactions with incoming ligands. A trigonal prismatic coordination is achieved by addition of two OH groups in the yz plane. As shown in Figure 1, the main interaction occurs between the metallic FMO $1b_2$ with the oxygen lone pair orbital $1b_2$. This interaction is strongly attractive because the antibonding component is pushed to high energy and vacated. The occupation of the metallic FMO $1b_2$ is 0.49 electron, while that of the oxygen orbital $1b_2$ is 1.80 electrons. This bonding is somewhat reinforced by a second bonding interaction between the bis(allyl)rhodium $3a_1$ orbital and the hydroxyl $1a_1$ orbital.

The large energy difference between these two orbitals prevents a significant interaction. A net rhodium-oxygen overlap population of 0.25 is computed for an 18-electron count. This particular electron count is favored since it leads to a HOMO-LUMO gap of 2.35 eV.

These results are expected for trigonal prismatic d^6 ML_6 coordination.[12] The rhodium d levels of **4** which are enclosed in a dashed box in Figure 1 may be identified with the typical level pattern obtained for a D_{3h} trigonal prism d^6 ML_6, i.e. three occupied MO's a'_1 and e' (which become $a_1(x^2-y^2)$, $a_1(z^2)$ and $b_1(xz)$ in the C_{2v} symmetry) and two high-lying vacant orbitals, e'' (becoming $a_2(xy)$ and $b_2(yz)$). Notice that the computed net charge of the rhodium center is quite positive (+2.28), while the one of the oxygen atoms of the hydroxyl groups is highly negative (-1.15). Consequently the bonding between the metal and the oxygen atoms is partly covalent, partly ionic.

The "square pyramid" model, $Rh(C_3H_5)_2(OH)$

If the bis(allyl)rhodium species is bound to only one oxygen atom from the TiO_2 surface, a 16-electron d^6 Rh(III) complex is attained. Basically the oxo-bis(allyl)rhodium species describes a square pyramid, the two allyl ligands constituting the basal plane and the oxygen atom occupying the apical site. Therefore we consider the electronic structure of the 16-electron d^6 Rh(III) model $Rh(C_3H_5)_2(OH)$, 6. Previous studies on square pyramidal ML_5 complexes[13] remind us that for large values of the angle θ (defined in 6) a d^8 18-electron complex is preferred.

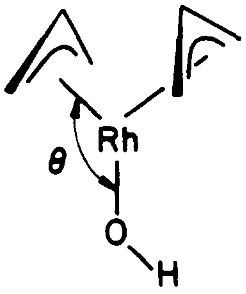

6

The orbital interaction diagram between $[Rh(C_3H_5)_2]^+$ and $(OH)^-$, illustrated in Figure 2, shows that the rhodium bonding occurs primarily through interaction of the σ lone pair orbital 1a' of the OH group with the metal s,z hybrid, 4a'($3a_1$ in C_{2v} symmetry). An important overlap between these orbitals compensates for a large energy difference. The population of the

Figure 2 here

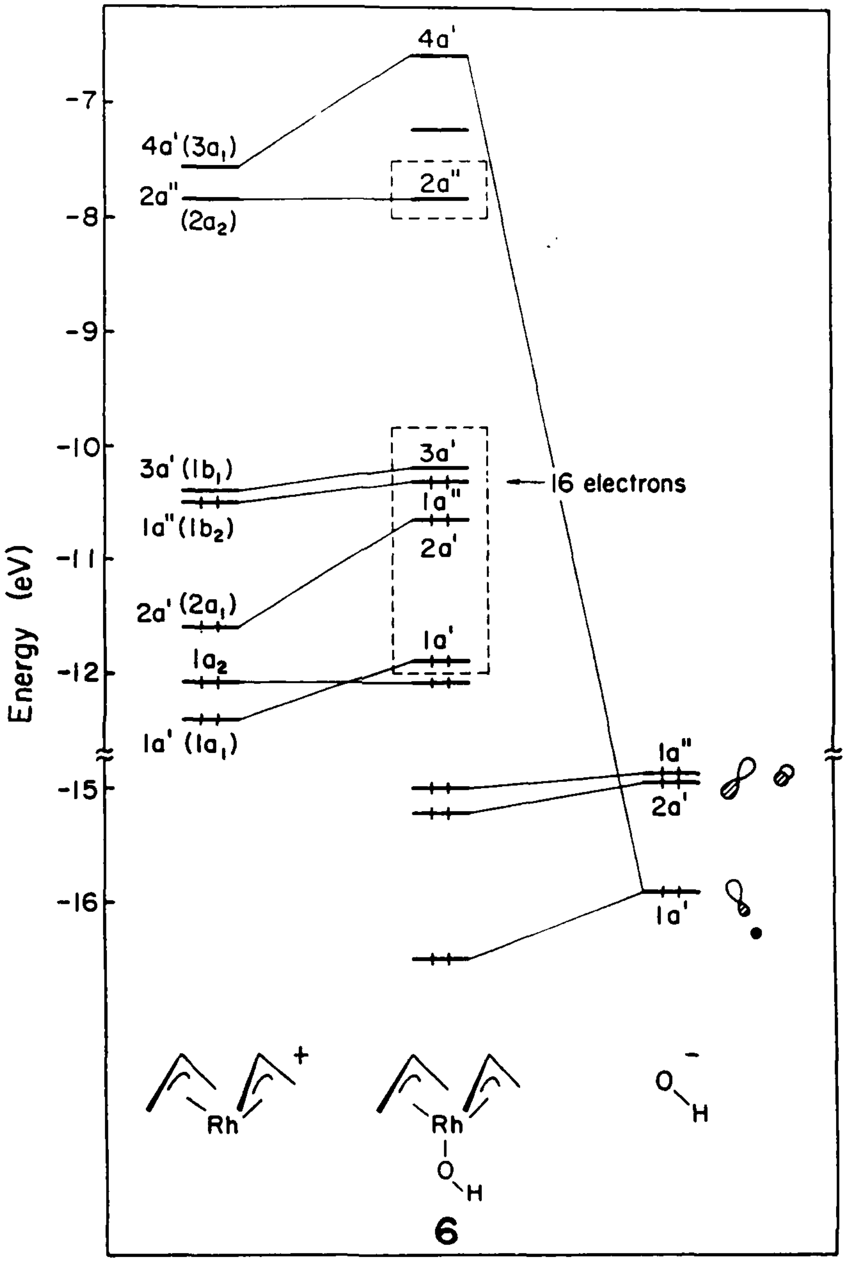

Figure 2. Interaction diagram for Rh(allyl)$_2$(OH).

4a'($3a_1$) FMO is 0.25 electrons after interaction. There is some interaction, to a lesser extent, between the metal 3a'($1b_1$) FMO, mainly xz, and one of the oxygen p orbitals, the orbital 2a'. This interaction is attractive for a 16-electron count. 0.06 electrons are transferred to the metallic 3a' FMO. The calculated metal-oxygen overlap population is 0.24 for a 16-electron count, quite similar to the one observed in 4.

For Rh(C_3H_5)$_2$OH, 6, the electron count is 16. The electronic structure of such a species does not appear attractive, since the HOMO 1a" (mainly yz) and the LUMO 3a'(xz) are nearly degenerate. An opening of the angle between the normals of the allyl ligands, which would favor the 16-electron count,[13] is unlikely in the present case. This would lead rapidly to steric hindrance with the surface support. On the other hand, an 18-electron count looks much better. The HOMO-LUMO gap is then 2.40 eV. The two additional electrons are housed in the 3a' MO. This orbital, drawn below in 7, is slightly rhodium-oxygen antibonding, and strongly rhodium-allyl

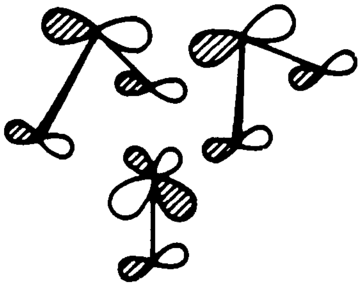

7

antibonding. Its occupation leads to a small decrease in the rhodium-oxygen overlap population (0.18 vs. 0.24), but mainly affects the rhodium-carbon(allyl) overlap population. The Rh-C(terminal) and Rh-C(central) populations were both 0.13 for the 16-electron complex. They are 0.07 and 0.06, respectively, if two electrons are added. The negative charge of the terminal carbon atoms of the allyl ligands increases from -0.32 (16 electrons) to -0.44 (18 electrons). It was -0.32 in the case of model **4**. These results are important when we think that an electrophilic attack by H^+ on the complex must occur.

The $Rh(C_3H_5)(H)(OH)_n$ models (n=1,3)

As we noted above, when the bis(allyl)rhodium complex is reacted with hydrogen, propene is produced and a new oxide-bound rhodium(allyl)(H) is formed. Here again, the question which arises is how the Rh(allyl)(H) moiety bonds to the inorganic support. The Rh(allyl)(H) fragment is basically a d^7 pyramidal ML_3 entity (close to the $Mn(CO)_3$ fragment of C_{3v} symmetry). At least three different ways of ligation to the surface may be envisaged. If the link is to one oxygen atom alone, a 14-electron tetrahedral ML_4 complex is obtained. A 16-electron square pyramidal ML_5 coordination results when the Rh fragment binds to two oxygen atoms. Anchoring to three oxygen sites leads to an 18-electron octahedral ML_6 species. In each case the Rh oxidation state of III is kept.

Let us concentrate now on different molecular models which mimic these three conceivable coordinations. The MO diagram of the model $Rh(C_3H_5)(H)(OH)$, 8, is shown in Figure 3, obtained by

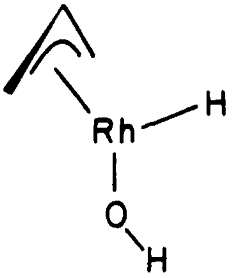

8

interaction of the ML_3 d^6 $[Rh(C_3H_5)(H)]^+$ moiety with an OH^-

Figure 3 here

group. The level scheme is reminiscent of the one observed for a distorted tetrahedral ML_4 complex with D_{2d} symmetry[11] (levels boxed by a dashed line in Figure 3). It appears that two electron counts are possible: 14 or 18. For a 14-electron species, most of the Rh-O bonding comes from the attractive interaction between the oxygen p orbital, 2a', of the hydroxyl group and the metallic 3a' orbital of the ML_3 fragment. 0.41 electrons are transferred to the metal FMO after interaction. This bonding is enhanced by interaction of the high-lying s,z hybrid of the metallic entity with the σ lone pair of the OH group. An overlap population of 0.29 is computed between the Rh center and oxygen atom, somewhat greater than the one calculated for 4 (0.24). A gap of 1.7 eV separates the HOMO 2a' from the LUMO 2a".

A stable 16-electron complex appears unreasonable since the 2a" and 3a' orbitals are nearly degenerate. On the other hand a gap of ca. 3 eV is secured if four rather than two electrons are added. Indeed the two orbitals 3a' and 2a" lie in the middle of a large energy gap. Their occupation, particularly that of 3a', leads to a significant diminution of rhodium-oxygen bonding. The Rh-O overlap population drops to 0.18. Because of the metal-ligand antibonding character of these orbitals, the Rh-C(allyl) bonds are also drastically weakened.

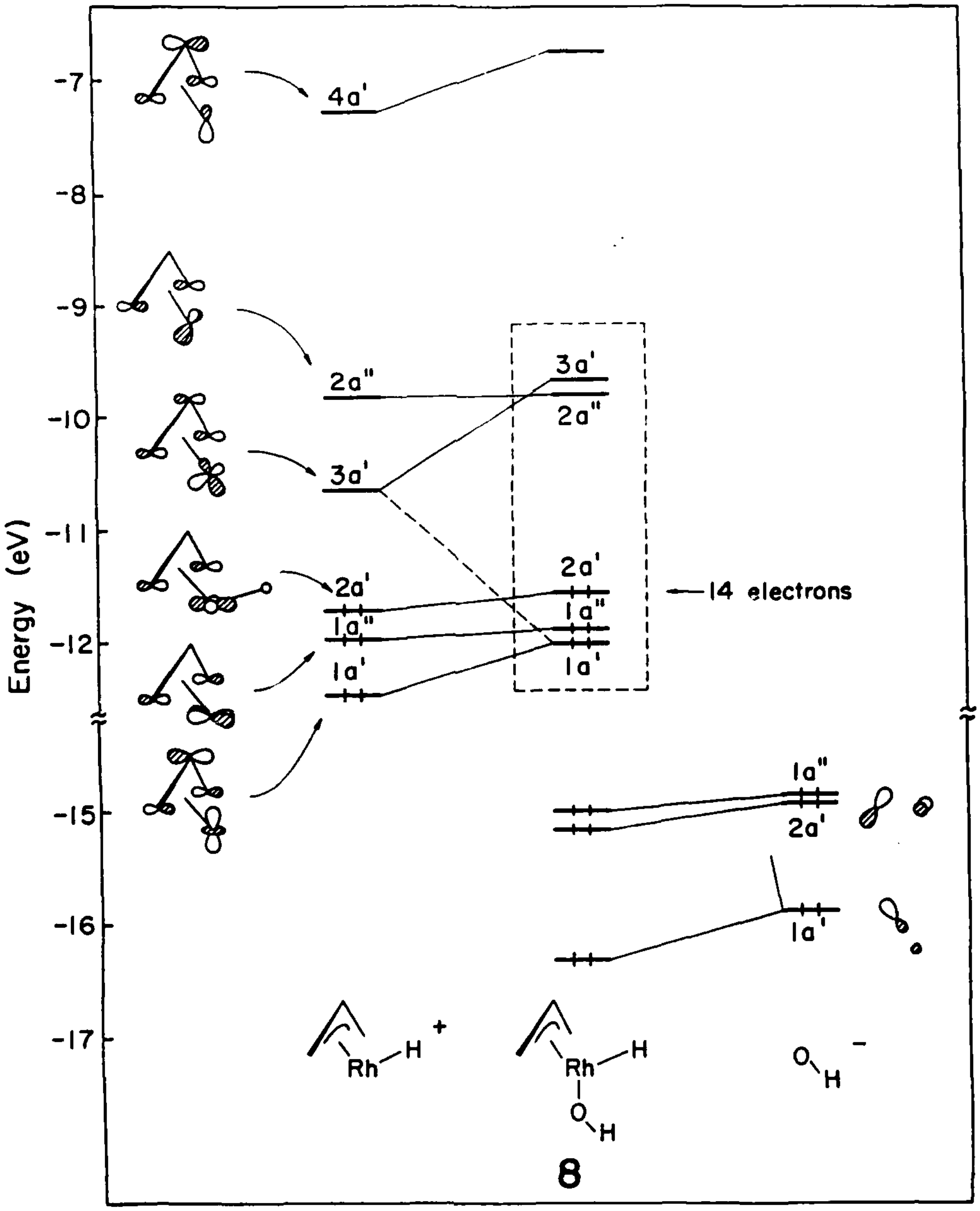

Figure 3. Interaction diagram for Rh(allyl)(H)(OH).

Let us mention that the $Rh(C_3H_5)(H)(OH)$ model complex, 8, exhibits the properties required of a reactive species for heterogeneous catalysis, i.e. significant Rh-O bonding insuring its immobilization over the organic support, and the presence of MO's in the middle of a large energy gap, allowing interesting reactivity. These are able to play either a donor or acceptor role.

The MO diagram of 9 in which the rhodium atom is attached to two oxygen atoms is shown in Figure 4. The MO pattern expected

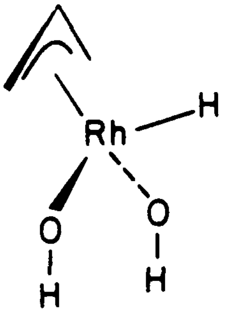

9

Figure 4 here

for a distorted square pyramidal ML_5 system[11] is somewhat perturbed due to the heterogeneity of the ligands. Nevertheless, it is possible to recognize the five predominantly metal d MO's in the HOMO-LUMO region (those boxed by a dashed line in Figure 4). The two upper MO's namely 2a" and 3a', interact strongly, with the out-of-phase and the in-phase combination of the σ lone-pairs of the hydroxyl groups, respectively. 1.64 eV separate the

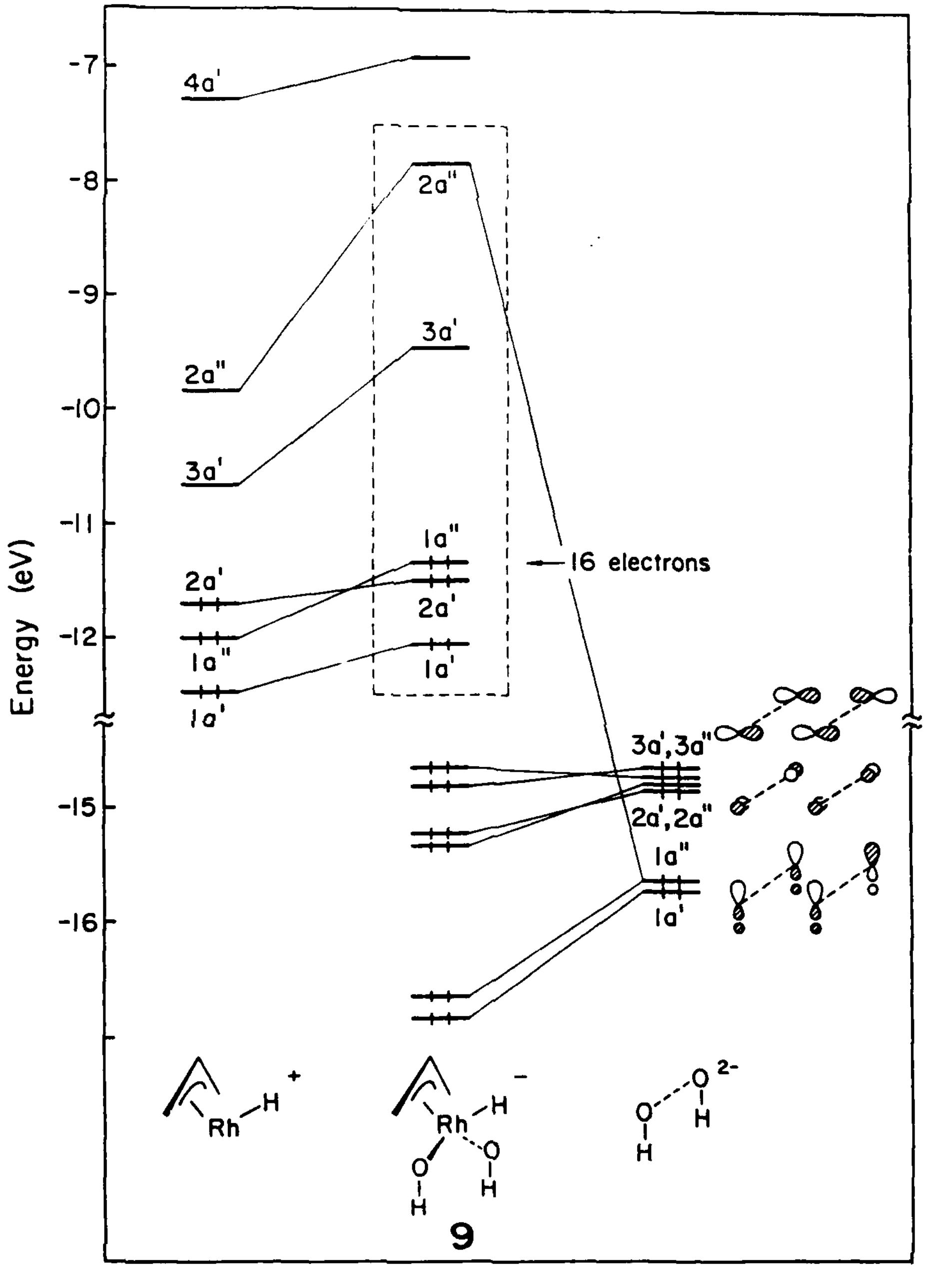

Figure 4. Interaction diagram for $[Rh(allyl)(H)(OH)_2]^-$.

resultant molecular orbital, 3a', from the upper 2a" MO, 1.79 eV from the lower-lying 1a" MO. Here again, two electron counts are possible, 16 or 18. For a 16-electron species, the computed rhodium-oxygen overlap population of 0.27 is quite comparable to the one calculated previously for the other models. The bonding between the allyl ligand and the rhodium atom is important (Rh-C(central):0.11; Rh-C(terminal):0.20). Population of the ligand-rhodium antibonding MO 3a' to attain an 18-electron count reduces the metal-ligand bonding somewhat. The Rh-O overlap population drops to 0.23, the Rh-C(central) and Rh-C(terminal) ones to 0.08 and 0.11, respectively. The overlap population between the rhodium atom and the hydride ligand diminishes as well (0.57 vs. 0.47). It is apparent that 9, like 8, may be a reactive species.

What remains is to look at the case where the $[Rh(allyl)(H)]^+$ fragment is attached to three oxygen atoms, 10.

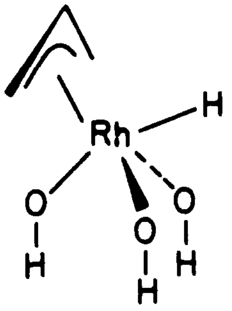

10

The relevant interaction diagram is not shown here, but it is typical of a saturated 18-electron system. There is a typical octahedral level splitting pattern, and a large gap (3.47eV) between HOMO and LUMO. There is strong Rh-O bonding. Such a complex is expected to be inert.

The fragment M(allyl)(H) is scarcely encountered in organometallic complexes. A 16-electron species, Ni(allyl)(H)(PR_3) has been mentioned some time ago.[14]

To sum up the results of our molecular models, the most reactive model species (the ones we are looking for) are the following: the 16-electron model **6** where the Rh(C_3H_5)$_2$ fragment is attached to one oxygen atom, the 14-electron model **8** and the 16-electron model **9**, the Rh(C_3H_5)(H) fragment being anchored to one and two oxygen atoms respectively.

Let us see now, how the features of the discrete model molecules translate into the interaction of metallic fragments with an inorganic surface support, the hydroxylated TiO_2 rutile (011) surface.

Electronic properties of the inorganic support

The rutile form of titanium dioxide TiO_2 crystallizes in a tetragonal lattice, 11. Each titanium atom is surrounded by a slightly distorted octahedron of oxygen atoms, and every oxygen atom is bonded to three metal atoms. The shortest O...O and Ti...Ti separations are substantial, 2.52 and 2.959Å respectively; thus there is no significant oxygen-oxygen or titanium-titanium interaction in the crystal, and localized octahedral bonding is maintained.[15] Rutile TiO_2 is a wide band-gap semiconductor; the experimental band-gap is 3.05eV.[16]

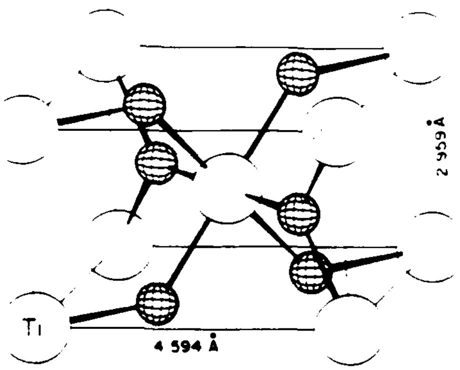

11

Rutile TiO_2 does not cleave well. Nevertheless, vacuum-fractured (100), (110) and (001) single-crystal surfaces have been studied.[17] It is firmly established from photoemission measurements that the electronic structure of the defect-free surfaces is essentially indistinguishable from that of the bulk, whatever the topology of the surface. This is surprising given that the local environment of the surface titanium is different according the face considered. For instance, the surface Ti atom on the (001) face is surrounded by only four oxygen atoms, compared to five or six in the (110) face or six in the (100) face. The absence of surface states in the bulk band gap has been confirmed by recent theoretical studies on the ideal TiO_2 (110), (100) and (001) surfaces.[18] Our calculations, performed on the TiO_2 (001) surface, chosen by Bernasek, Schwartz and colleagues for their investigations, show the same results. Reduction of the coordination of Ti atoms is not in itself sufficient to alter surface electronic structure. Both experimental and theoretical studies agree that oxygen vacancies are necessary to induce occupied surface states in the bulk-band gap region.[17,19-20]

Although the ideal TiO_2 (001) surfaces does not present dangling-bond surface states in the band-gap region, the surface is unstable. It facets on annealing to produce a (011) (2x1) structure.[21] The atomic geometry of the structure is not fully understood, so an ideal TiO_2 (011) surface has been considered for the calculations. The surface Ti atom of a clean (011) surface is surrounded by five oxo-ligands. Our calculations indicate that the electronic structure of this surface is quite comparable to the one of bulk TiO_2. No surface states appear in the bulk band-gap region.

Metal oxide surfaces usually react with water. The important question is whether the adsorption of H_2O is molecular or dissociative. Despite numerous studies, the nature of the adsorption of water on rutile TiO_2 surfaces is still controversial.[17,22] Smith and Bernasek have observed that H_2O adds dissociatively on TiO_2 (011) surface[23] to form two types of surface hydroxyl groups: monodentate and bidentate (12). The surface can be fully hydroxylated since there is one surface

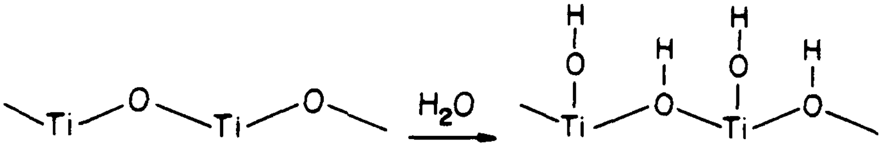

12

titanium atom for every protruding oxygen atom. These hydroxyl groups are necessary for the reaction with Rh(allyl)$_3$ to occur. Upon heating some OH groups desorb but as their number is not known, we considered a fully hydroxylated model. Moreover, our model was defect-free, although the dark blue color of the TiO_2 sample used for the experimental investigations is characteristic of a non-stochiometric material.

The rectangular unit cell of the hydroxylated TiO_2 (011) surface is depicted in 13. The hatched atoms come from water molecules which have been dissociated. Only one layer is shown for clarity in the top view (three layers were used for the computations; see Appendix for other computational details). Upon hydroxylation, every surface titanium atom, which was five-coordinated in the bare surface, has restored its octahedral environment. Therefore the analysis of the electronic structure of the surface is fairly simple. Its total density of states is

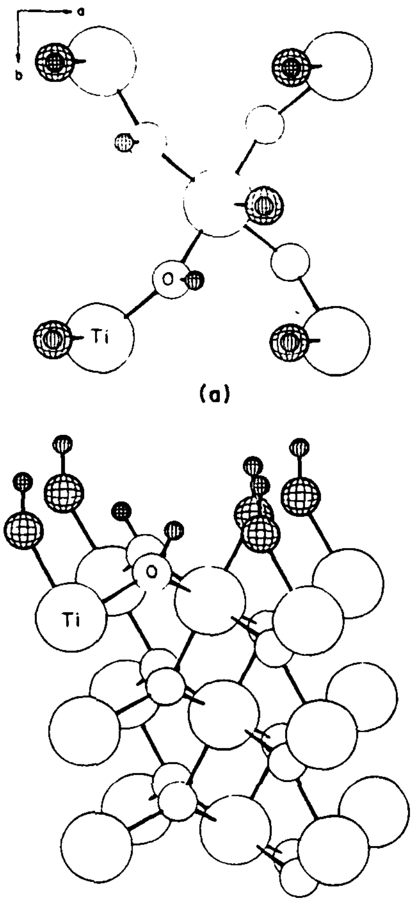

(a)

(b)

13

shown in Figure 5. Some explanation is necessary for what is

Figure 5 here

shown in this diagram. On moving from the discrete molecule to the solid or surface, each orbital of the molecule or unit cell generates a band of orbitals in the extended material.[24] The best way to look at this multitude of levels is to follow the density of states (DOS), i.e. the relative number of energy levels in a given interval. This is the curve plotted by a

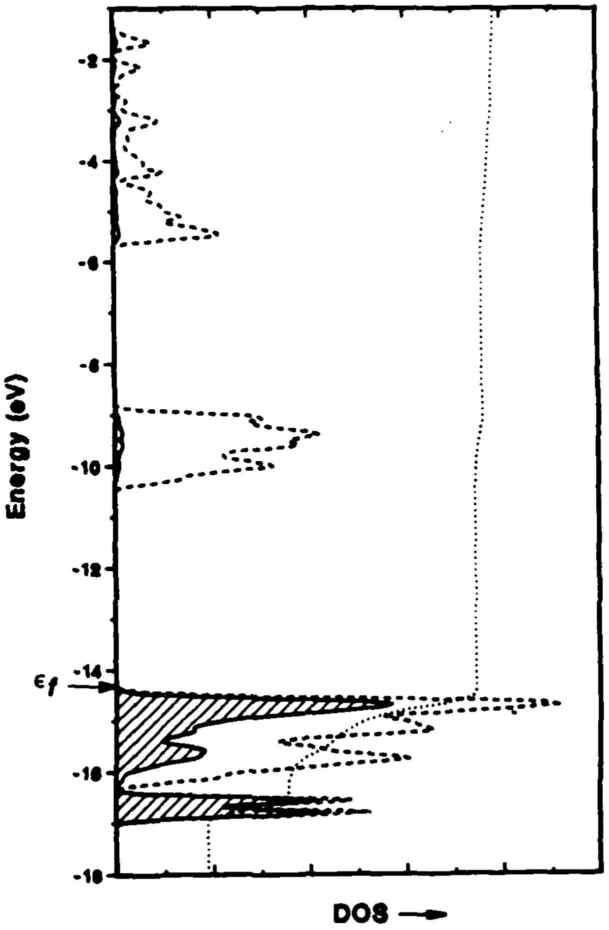

Figure 5. Total DOS (dashed line) and the hydroxyl contribution (lined area) of the hydroxylated TiO_2 (011) surface.

dashed line in Figure 5. It is quite analogous to that of bulk TiO_2[15] which is illustrated in Figure 6. In addition to the expected O 2s, O 2p, Ti t_{2g} and e_g bands (the low-lying O 2s band is not shown), there appears in Figure 5 a sharp doubled peak, made of oxygen-hydrogen bonding surface states at the bottom of the O 2p band. No surface states are found in the bulk band-gap. The hatched area indicates the contribution of the surface hydroxyl group states to the total DOS. This is an example of projected or local DOS curve that singles out the contribution of certain atoms or a group of atomic or fragment orbitals to the overall DOS plot. The dotted line is an integration curve, from 0 to 100%, which simply counts the relative number of states occupied as one sweeps up the energy scale. Note that the top of the valence band, the O 2p band, is derived mainly from the oxygen atoms of the hydroxyl groups. Both surface and bulk titanium atoms carry almost the same charge, +1.80 and +1.85, respectively. The charges of the oxygen atoms are between -0.72 and -1.00.

<u>Figure 6 here</u>

As noted experimentally, the oxygen atoms of the hydroxyl groups are firmly bound to the surface. Ti-O overlap populations of 0.40 and 0.47 are computed for bi- and mono-dentate hydroxyls respectively compared to 0.41 (average) for the bulk Ti-O bonds.

Generally, when oxides are exposed to a moist atmosphere the M-OH groups can dissociate (more or less reversibly) either as

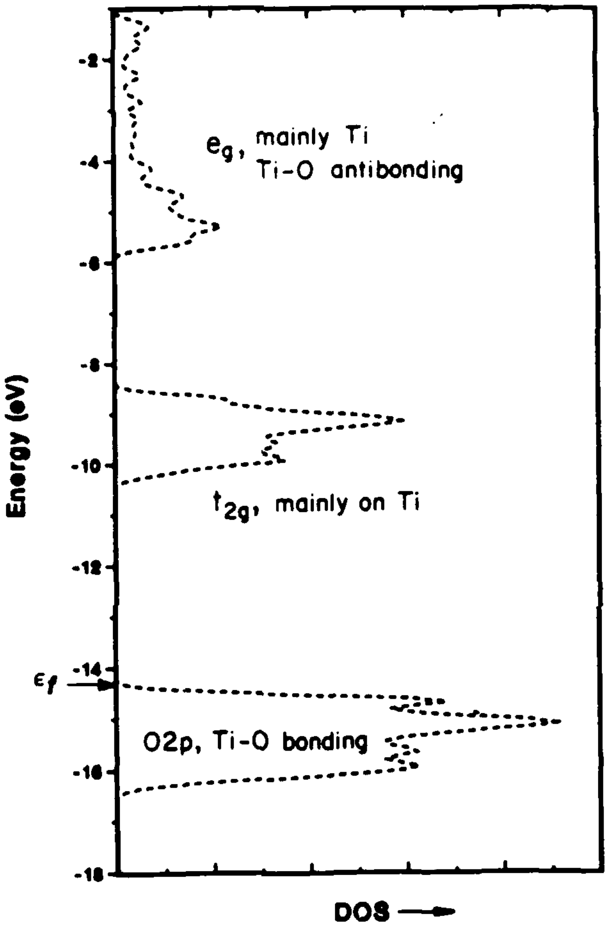

Figure 6. Density of states of TiO_2 bulk.

bases or acids, depending on the electronegativity of the atom M. For instance:

$$\text{Mg-OH} \longrightarrow \text{Mg}^{2+} + \text{OH}^- \quad \text{(I)}$$

$$\text{Si-OH} \longrightarrow \text{SiO}^- + \text{H}^+ \quad \text{(II)}$$

If the cation M is an electropositive element, M-OH dissociates to give hydroxyl anions (I). If M is more electronegative, M-OH dissociates to give protons (II). Hydroxylated rutile surfaces behave as hydroxylated silica (II). During this process, the protons can be exchanged with other cationic species, for example the organo-rhodium compounds. This property is exploited in the preparation of supported metal catalysts (Scheme 1). We can imagine simply that a liberated proton activates the organometallic precursor tris(allyl)rhodium. Propene is formed and the derivative bis(allyl)Rh cation is anchored to one or more oxygen atoms of the surface.

Adsorption of the $[Rh(C_3H_5)_2]^+$ fragment

According to Auger data[2], the ratio of adsorbed rhodium centers to surface titanium atoms is 1 to 4. This is the maximum coverage for which excessive steric hindrance between two organometallic species is avoided. The primitive unit cell contains two surface Ti atoms, so a super unit cell (011)-p(2x1) containing four surface Ti centers (9.188Å x 5.466Å) was considered by us. The larger unit cell plus the size of the adsorbate forced us to take a one-layer film instead of the three-layer one we used previously. Results obtained for the fully hydroxylated surface with three layers do not differ very much from those obtained with one layer since the surface appears to cause little perturbation of the DOS. One side of the film was covered by the adsorbate, the other side terminated by hydrogen atoms. As we did for the molecular models, we shall analyze the bonding of the bis(allyl)rhodium cation with one and two oxygen-active sites of the surface.

I. One-oxide-bound bis(allyl)rhodium species

When a proton from one hydroxyl group of the surface is expelled and activates the tris(allyl)rhodium complex, a two-electron oxygen anion is generated. This two-electron donor interacts with the electrophilic 14-electron species $[Rh(C_3H_5)_2]^+$ and a 16-electron system is achieved. The active oxygen center can be either Ti-Ti bridging or terminal-bound to titanium. We chose to look at the system where the rhodium fragment is attached to a terminal oxygen atom (A) since the other (B) is already two-coordinate and buried into the surface, less accessible to the bulky Rh adsorbate (see **14**; the atoms of the $Rh(allyl)_2$ fragment are hatched).

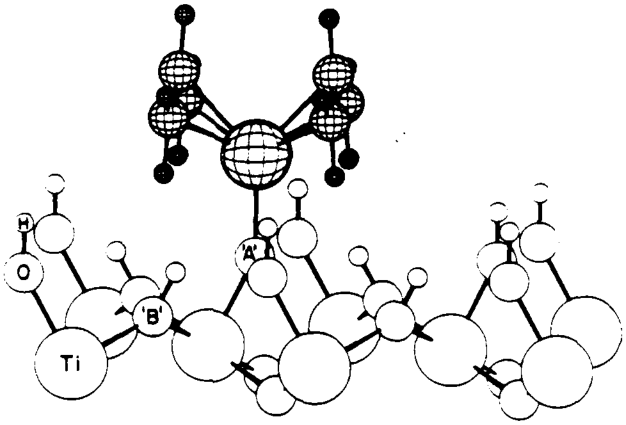

14

We show in Figure 7 the "interaction diagram" for $[Rh(C_3H_5)_2]^+$ bound to one oxygen atom of hydroxylated TiO_2 (011)

Figure 7 here

surface. In Figure 7c, the energy levels of an isolated $[Rh(C_3H_5)_2]^+$ fragment spread out into the bands of a $\{[Rh(C_3H_5)_2]^+\}_\infty$ layer. Of course the bands are narrow, because the organometallic fragments are far away from each other. The MO's of an isolated fragment are drawn as bars on the far right.

On the left side of the Figure, in Fig. 7a, is the DOS of the rutile (011) surface by itself. The detective work of tracing orbital interactions is facilitated by following decompositions of the total DOS, atom by atom, or orbital by orbital. For instance the lined area in Figure 7a shows the

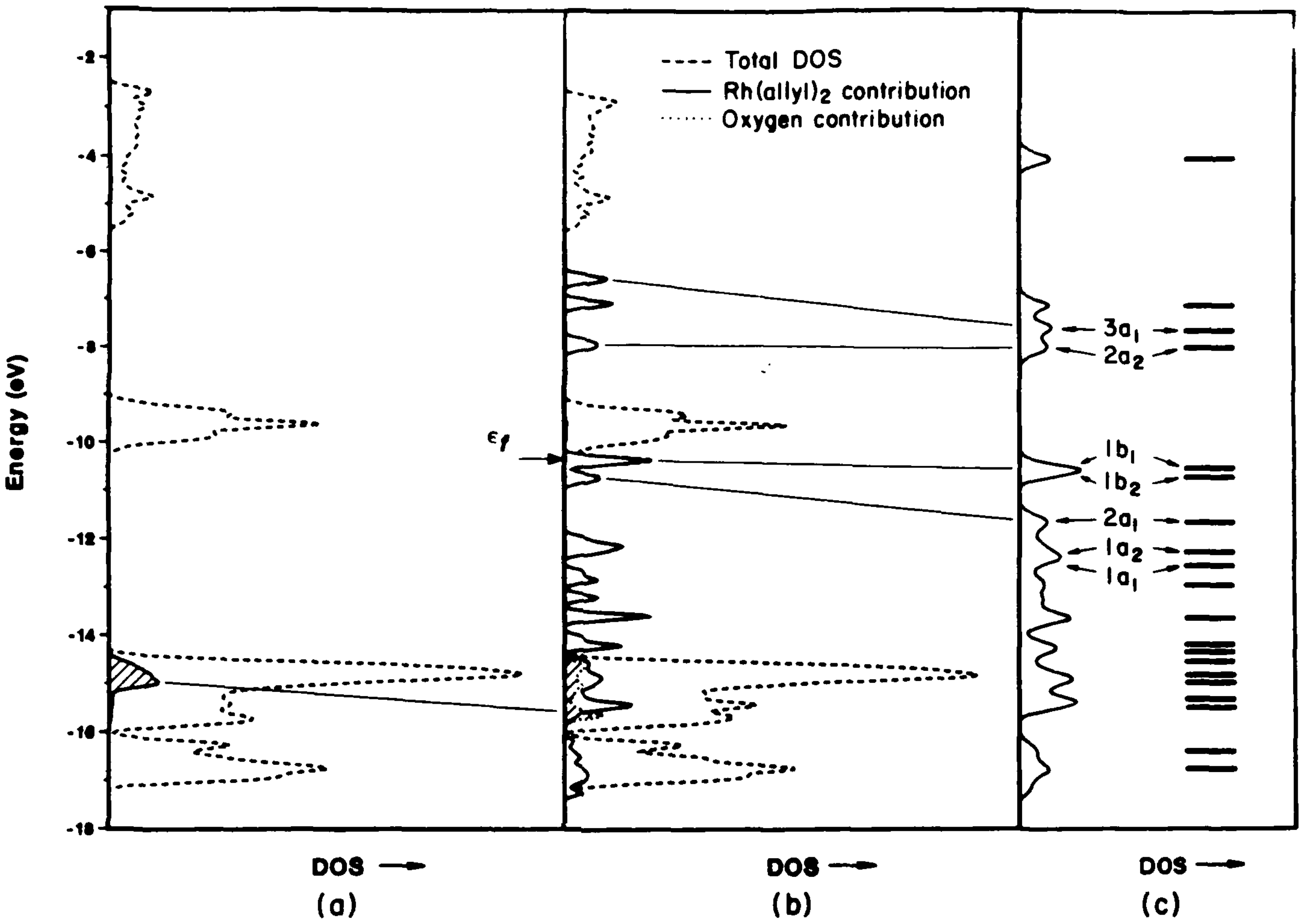

Figure 7. (a) Total DOS (dashed line) and active oxygen contribution (lined area) for hydroxylated TiO_2 (011) support before interaction.

(b) Total DOS (dashed line), active oxygen (lined area) and bis(allyl)Rh (solid line) contributions when bis(allyl)Rh is linked to one oxygen atom from hydroxylated TiO_2 (011) support.

(c) Total DOS for the bis(allyl)Rh layer before interaction. The sticks refer to the MO's of an isolated bis(allyl)Rh fragment.

contribution to the total DOS of the rutile oxygens to which the Rh fragments will be bound. It is this DOS which we expect to be most affected by binding Rh.

The middle panel, Figure 7b, shows the DOS of the composite, rutile $Rh(C_3H_5)_2$ system. The dashed line appears to be a simple superposition of the left and right panels, the separate components. Differences (that is where bonding, repulsion are) are traced by the above-mentioned decompositions of the DOS. Thus the solid line in Figure 7b is the contribution of $[Rh(allyl)_2]^+$ FMO's to the DOS of the composite system, and the lined area is that of the active oxygen of the surface support.

There are some changes, indicative of bonding. Note the active oxygen DOS is quite perturbed by the Rh. Correspondingly the Rh fragment a_1 levels are pushed up. We have drawn lines connecting matching electron density peaks. These lines have the same meaning — interaction — as they do in a molecular interaction diagram (see 15).

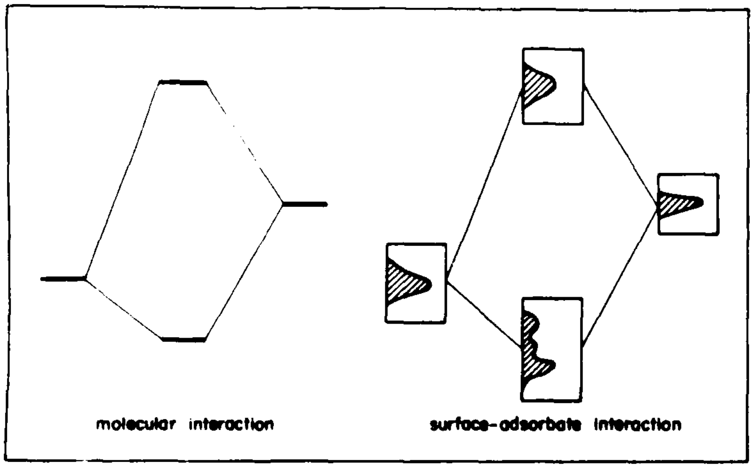

15

Overall, the situation encountered is reminiscent of the one observed for the molecular model 6, $Rh(C_3H_5)_2OH$. The major bonding interaction occurs between the σ lone pair of the oxygen of the surface and the high-lying FMO $3a_1$ from the bis(allyl) rhodium fragment. From the comparison of Figure 7a and Figure 7b, it emerges that the electronic structure of the inorganic support is almost unperturbed after chemisorption of the organometallic species. Only the band due to the oxygen atom linked to the rhodium fragment is spread out after interaction. For instance, upon looking at the inactive oxygen or titanium contributions to the DOS, which we have done but now shown in Figure 7, we find almost no change from the isolated hydroxylated surface. Thus, the bonding of the adsorbate with the adsorbent is essentially localized between the rhodium center and the oxygen of the support. The effect of the adsorption on the rest of the metal oxide surface seems extremely weak. The charge carried by the titanium atom attached to the active oxygen does not change more than 5 percent from the other surface titanium atoms.

Though the bonding description is very similar to that in the isolated complex 6, there is one difference in the surface case. In the molecular case, the two FMO's $1b_1$ and $1b_2$ are quite close in energy after interaction with the OH group (see Figure 2). For a 16-electron complex, $1b_2$ (1a") is occupied and $1b_1$(3a') is vacant. In the case of the surface, these two FMO's generate two narrow bands which, after interaction with the inorganic support, are almost at the same energy around the Fermi level. The overlap of these two narrow bands leads to a depopulation of the band derived from $1b_2$ FMO and a partial population of the band derived from the $1b_1$ orbital (see Table 1). This is shown schematically in 16. The actual populations of $1b_2$ and $1b_1$ orbitals are 1.21 and 0.55 respectively, after interaction, vs. 2.00 and 0.06 in the case of the molecular model 6. This does not strongly affect the overall bonding between the rhodium atom and its ligands. Actually the two bands are metal-ligand antibonding. Therefore, the bonding gained by depopulation of one band is lost by population of the other. So the computed overlap population between the rhodium center and oxygen atom and the allyl groups are similar to those for 6 (see Table 1).

Table 1 here

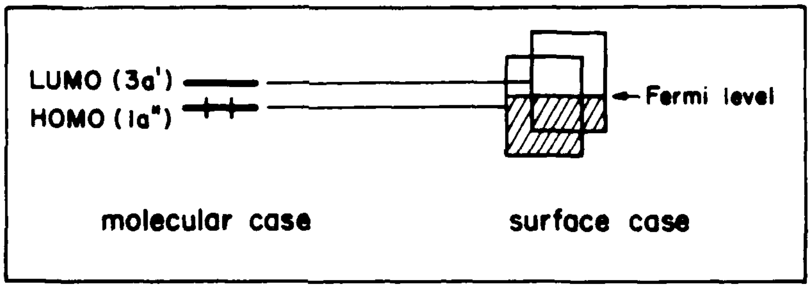

16

Table 1. Binding characteristics of the one-oxide-bound bis(allyl)Rh species.

MO net occupations of the $Rh(C_3H_5)_2$ fragment	$Rh(C_3H_5)_2$ on surface	$Rh(C_3H_5)_2(OH)$ 16 electrons	$Rh(C_3H_5)_2$ on reduced surface	$[Rh(C_3H_5)_2(OH)]^{2-}$ 18 electrons
$1a_1$ (1a')	1.93	1.93	1.93	1.93
$2a_1$ (2a')	1.87	1.88	1.87	1.89
$1b_2$ (1a")	1.21	2.00	1.71	2.00
$1b_1$ (3a')	0.55	0.06	1.29	2.00
$3a_1$ (4a')	0.25	0.25	0.25	0.25
Overlap populations				
Rh-O	0.27	0.25	0.22	0.19
Rh-C(central)	0.11	0.13	0.06	0.06
Rh-C(terminal)	0.13	0.13	0.08	0.07

II. More electrons

Upon reduction, TiO_2 rutile becomes an n-type semiconductor and its color changes from clear yellow to opaque blue. This is the actual color of the TiO_2 sample used in the experiments. That means some of the 3d levels of the titanium atoms (surface and/or bulk) are partially populated. There are several possibilities for reducing TiO_2. It may be doped by small atoms (H, Li, Cr) which diffuse along the open "channels" present in the structure.[25] At relatively high temperature, addition of H_2 leads to formation of water and microdomains of Ti_2O_3.[16,26] Oxygen vacancy defects are created by Ar-ion bombardment. The exact nature of these vacancies has been studied recently, both experimentally[17] and theoretically.[19] Reduced TiO_2 surfaces exhibit occupied states of 3d Ti parentage in the bulk band-gap region at about 0.7-0.8 eV below the bottom of the conduction band.

We choose to simulate the reduced hydroxylated surface by injecting a small number of electrons in the unit cell. Adding two electrons per cell gives formally $3d^{0.125}$ Ti surface atoms. These extra electrons are housed in the bottom of the conduction band, the Ti 't_{2g}' band. Let us examine now how the bonding between the bis(allyl)Rh species and the metal oxide surface is affected by this extra electron population. A glance at the Table 1 shows a significant change in the rhodium-oxygen bonding (a decrease of 19%). Now the $1b_2$ and $1b_1$ levels of the bis(allyl)rhodium fragment are both occupied after interaction with the oxygen of the support (see Table 1). These levels, being strongly ligand-metal antibonding, force the Rh-O and Rh-C (allyl) overlap populations to drop quite substantially, particularly the Rh-allyl one, rendering the allyl ligand more vulnerable to a possible electrophilic attack. Recall that we saw a similar result when we added two electrons to the 16-electron model 6, $Rh(C_3H_5)_2(OH)$. Population of the ligand-rhodium antibonding component deriving from the interaction of the $1b_1$ level with the surface is due to its position in the DOS, just underneath that of the partially filled conduction band of TiO_2 surface. This is sketched in 17; the bonding two-electron-two-orbital interaction present in the molecular complex **17a** is replaced by an antibonding four-electron-two-orbital interaction for the surface (**17b**). This situation is often encountered in the case of metallic surfaces.[5b]

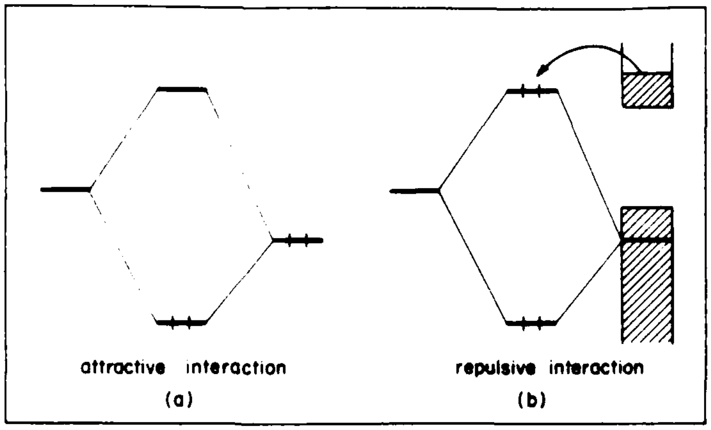

17

Though the electronic transfer from the surface toward the rhodium species must weaken the ligand-metal bonding, it allows the ML_5 adsorbate to satisfy its 18-electron requirement.

III. Two-oxide-bound bis(allyl)rhodium species

The 16-electron one-oxide-attached bis(allyl)rhodium(III) adsorbate can easily bend toward an adjacent terminal hydroxyl group and bind to it through a p-type lone pair. The formal oxidation state of III is retained and an 18-electron prismatic ML_6 species is formed (see 18). Here again the bonding between the rhodium center and the two oxygen atoms is quite comparable to that observed for the molecular complex model $[Rh(C_3H_5)_2(OH)_2]^-$, **4** (compare Figure 1 and Figure 8).

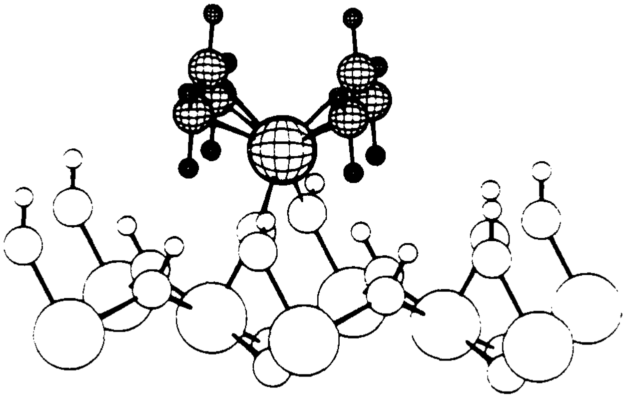

18

Figure 8 here

The allyl-rhodium antibonding $1b_2$ FMO is found vacant, high above the Fermi level after interaction with the σ orbitals of the two oxygen atoms. On the other hand the $1b_1$ orbital is occupied (see Table 2). The occupation of this orbital, being localized on the central carbon atom of the allyl units (see Figure 1) explains the rather large difference between the

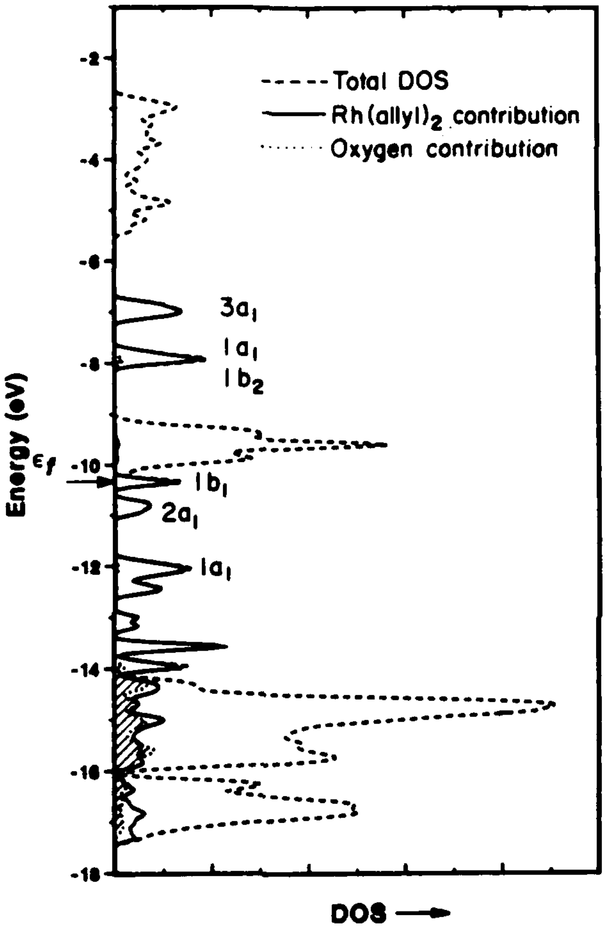

Figure 8. Total DOS (dashed line), Rh(allyl)$_2$ contribution (solid line) and oxygen contribution (lined area) when Rh(allyl)$_2$ is linked to two oxygen atoms of the hydroxylated TiO$_2$ support.

Table 2 here

Rh-C(terminal) and Rh-C(central) overlap populations (0.12 vs. 0.06). Contrary to the one-oxygen-bound species no change is observed in Table 2 for the bonding between the organometallic adsorbate and the oxide adsorbent when the latter is reduced. All the organo-rhodium levels lying between the valence band and the conduction band of the oxide support are filled. Therefore no electron flow occurs from the titanium 't_{2g}' band towards the organo-rhodium adsorbate.

Let us sum up the results we obtained for the anchoring of the bis(allyl)rhodium entity on the TiO_2 inorganic support. Both types of ligated species, one-and two-oxide-bound complexes appear to be stable on the surface. Intuitively, a more reactive species will serve as a better intermediate for the continued reaction, thus our preference goes to the single-oxide-bound organo-rhodium complex on a reduced oxide surface. The small number of electrons stored in the titanium 't_{2g}' band can pour into the allyl-rhodium antibonding levels, leading to a weakening of the carbon-rhodium bonds, particularly the carbon(terminal)-rhodium one. The weakening of that bond is a necessary step in the formation of propene and the (allyl)rhodium hydride adduct. Depopulation of the Ti 't_{2g}' reservoir does not seem to affect the bonding in the oxide support.

Table 2. Binding characteristics of the two-oxide-bound bis(allyl)Rh species.

MO net occupations of the $Rh(C_3H_5)_2$ fragment	$Rh(C_3H_5)_2$ on surface	$[Rh(C_3H_5)_2(OH)_2]^-$ 18 electrons	$Rh(C_3H_5)_2$ on reduced surface
$1a_1$	1.99	2.00	1.99
$2a_1$	1.87	1.88	1.88
$1b_2$	0.48	0.49	0.51
$1b_1$	0.98	2.00	1.74
$3a_1$	0.13	0.15	0.14
Overlap populations			
Rh-O	0.23 0.24	0.25	0.23 0.24
Rh-C(central)	0.06	0.05	0.06
Rh-C(terminal)	0.12	0.11	0.12

Adsorption of the $[Rh(C_3H_5)(H)]^+$ fragment

Let us proceed now to analyze the interaction of the catalytic species $Rh(C_3H_5)(H)$ with one, two or three oxygen atoms of the oxide surface.

I. Single-oxide-bound (allyl)rhodium hydride complex

The relevant FMO's of the (allyl)rhodium(H) entity before and after interaction with one oxygen atom of the inorganic support (see 19) are shown in Figure 9. There is no major difference between that figure and Figure 3, where the MO diagram of the molecular model $Rh(C_3H_5)(H)(OH)$ was shown. The main feature here is the resonance of some organo-rhodium levels with the conduction band of the oxide support. Actually, these organometallic states descend from the 3a' and 2a" FMO's. They are antibonding between the metallic atom and its ligands (see Figure 3). Their occupation would lead to a drastic change in

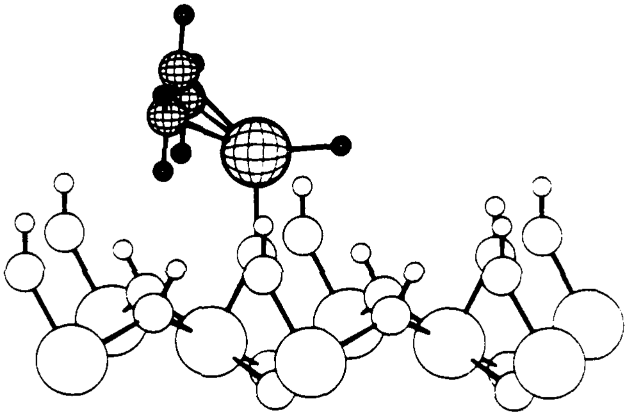

19

Figure 9 here

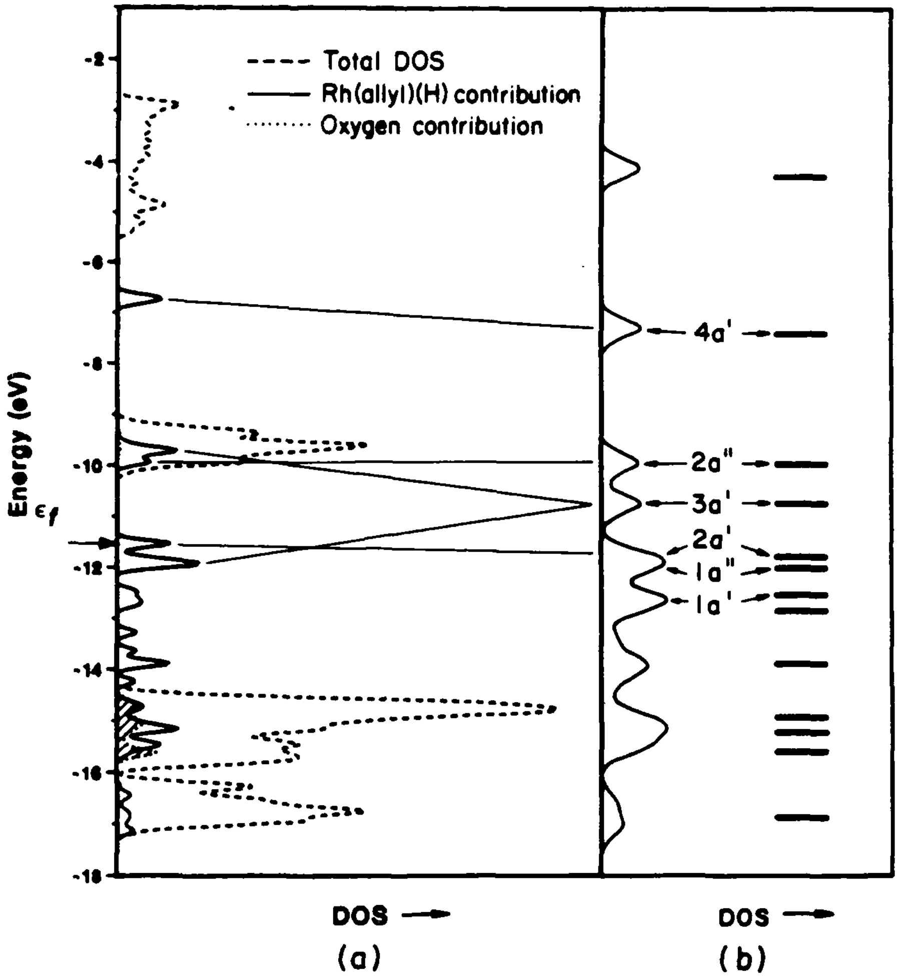

Figure 9. (a) Total DOS (dashed line), active oxygen (lined area) and Rh(allyl)(H) (solid line) contributions when Rh(allyl)(H) is linked to one oxygen atom from the hydroxylated TiO_2 support.
(b) Total DOS for the Rh(allyl)(H) layer before interaction. MO's of an isolated Rh(allyl)(H) group are shown on the far right.

the bonding between the rhodium center and its ligands, as we saw previously for the 18-electron molecular model $[Rh(C_3H_5)(H)(OH)]^{4-}$ (see table 3). According to the calculations, injecting a small number of electrons in the oxide conduction band is not sufficient to populate completely these organo-rhodium bands and thus to alter the ligand-rhodium bonding. These extra electrons are housed in the bottom of the conduction band. However, we do think that reduction of the inorganic support enhances the reactivity of the adsorbed species. Resonance of empty organo-rhodium states with the partially filled conduction band of the oxide surface allows electrons to move back and forth according to the electronic requirements of the adsorbate.

Table 3 here

A word of caution is necessary. The conclusions reached here are sensitive to the inadequacies of the extended Hückel method and our particular choice of a model for the reduced surface. It could be that our parameter set for Rh and rutile is deficient, and thus the relative position of the t_{2g} and 3a' and 2a" not realistically modelled. It could also be that simple filling of the t_{2g} band to model the reduced surface is inadequate, and that it is important to introduce real defects and their associated states below the conduction band.

Table 3. Binding characteristics of the one-oxide-bound Rh(allyl)(H) complex.

MO net occupations of $Rh(C_3H_5)(H)$ fragment	$Rh(C_3H_5)(H)$ on surface	$Rh(C_3H_5)(H)(OH)$ 14 electrons	$Rh(C_3H_5)(H)$ on reduced surface	$[Rh(C_3H_5)(H)(OH)]^{4-}$ 18 electrons
1a'	1.71	1.77	1.77	1.91
1a"	1.99	2.00	1.99	2.00
2a'	1.32	1.99	1.99	2.00
3a'	0.37	0.40	0.39	1.86
2a"	0.03	0.03	0.46	2.00
4a'	0.04	0.05	0.04	0.20
Overlap populations				
Rh-O	0.30	0.29	0.30	0.18
Rh-C(central)	0.09	0.10	0.09	0.10
Rh-C(terminal)	0.18	0.18	0.16	0.01
Rh-H	0.57	0.57	0.57	0.51

II. Two-oxide-bound (allyl)rhodium hydride complex

Bonding of the $[Rh(C_3H_5)(H)]^+$ fragment through one oxygen anion and one hydroxyl group of the support (20) gives a 16-electron Rh(III) complex. Indeed, we saw in Figure 4 that two electron counts were possible, either 16 or 18, since an MO derived from the 3a' FMO lies in the middle of a large energy gap. An identical situation is encountered for the surface case, as shown in Figure 10.

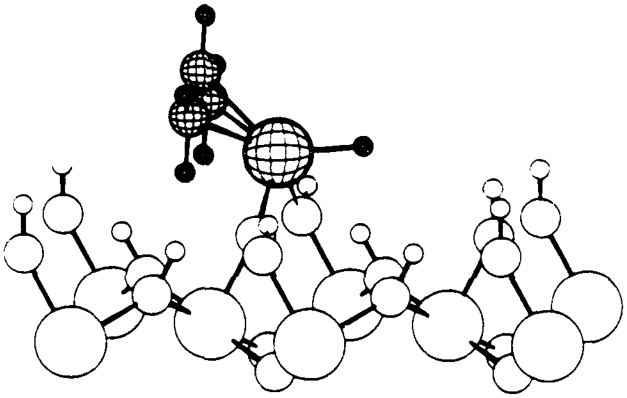

20

Figure 10 here

The Fermi level is positioned at the top of an organo-rhodium/surface band of 2a' and 1a" parentage. A glance at Table 4 shows that the binding characteristics of the surface case and

Table 4 here

the 16-electron molecular model case are quite comparable. We notice the presence of empty organometallic states derived from

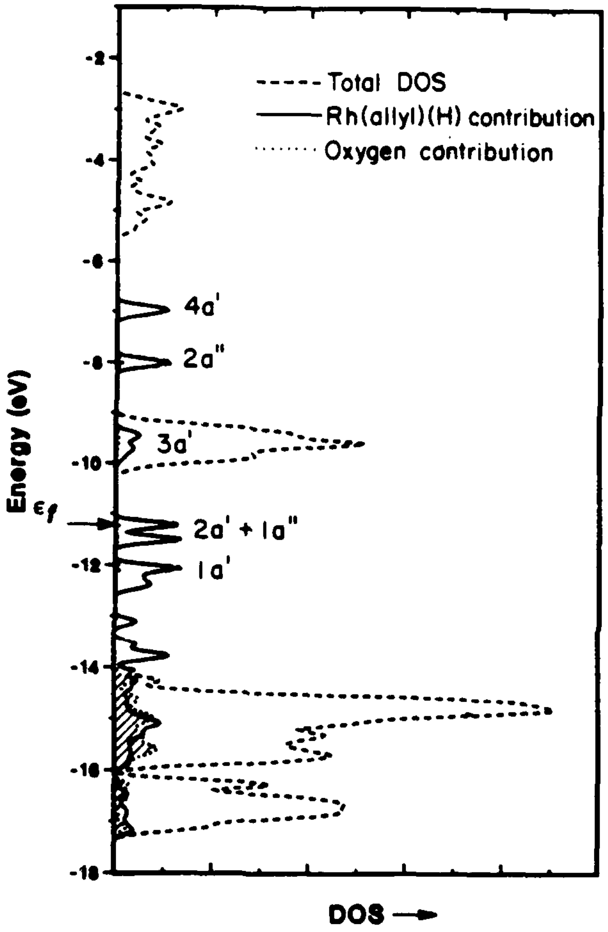

Figure 10. Total DOS (dashed line), active oxygen (lined area) and Rh(allyl)(H) (solid line) contributions when Rh(allyl)(H) is linked to two oxygen atoms from the hydroxylated TiO_2 support.

Table 4. Binding characteristics of the two-oxide-bound Rh(allyl)(H) complex.

MO net occupations of $Rh(C_3H_5)(H)$ fragment	$Rh(C_3H_5)(H)$ on surface	$[Rh(C_3H_5)(H)(OH)]^-$ 16 electrons	$Rh(C_3H_5)(H)$ on reduced surface	$[Rh(C_3H_5)(H)(OH)]^{3-}$ 18 electrons
1a'	1.98	2.00	1.98	2.00
1a"	1.57	1.88	1.87	1.88
2a'	1.59	1.90	1.87	1.97
3a'	0.26	0.30	0.35	1.82
2a"	0.41	0.56	0.52	0.56
4a'	0.02	0.02	0.03	0.13
Overlap population				
Rh-O	0.24 0.24	0.27	0.24 0.23	0.23
Rh-C(central)	0.11	0.11	0.10	0.08
Rh-C(terminal)	0.20	0.20	0.20	0.11
Rh-H	0.56	0.57	0.55	0.47

the 3a' FMO at the same energy as the oxide conduction band. Here again, as before, a slight reduction of the oxide support will not populate these empty adsorbate states. But we conclude, as in the previous case where the rhodium entity was attached to one oxygen atom, that a reduced oxide surface would help the reaction process. Population of these organometallic states would lead to a noticeable weakening of the bonding between the rhodium center and the terminal carbon atom of the allyl group and the hydrogen atom (see the binding characteristics of the 18-electron molecular model in Table 4).

III. Three-oxide-bound (allyl)rhodium hydride complex

An 18-electron Rh(III) species is attained when the rhodium atom is linked to one oxygen anion and two hydroxyl groups of the oxide surface. Calculations on the molecular ML_6 model $[Rh(C_3H_5)(H)(OH)_3]^{2-}$, 10, showed that a very stable complex could be obtained for such an electron count. Ligation of the $Rh(C_3H_5)(H)$ unit on the oxide surface through three oxygen atoms seems unlikely for steric reasons. As seen below in 21,

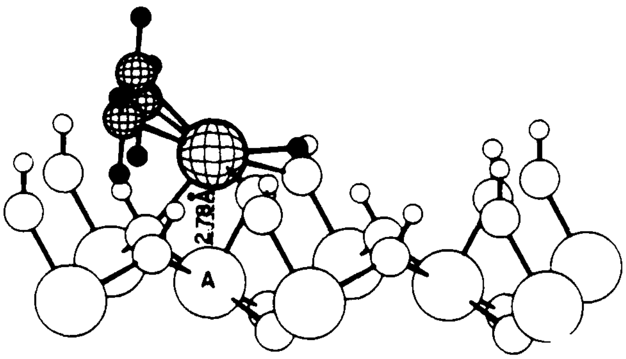

21

the rhodium(allyl)(H) fragment is buried in the oxide surface, producing some steric strain between the hydroxyl groups of the surface and the ligands of the rhodium center. Moreover, a short contact is created between the rhodium and one titanium of the surface (marked A in 21). When the imposed Rh-O distance is 2.0Å, the separation between Rh and Ti_A is only 2.78Å, clearly indicating metal-metal bonding. Bonding interaction between rhodium and titanium atoms has been observed when rhodium metal is dispersed on titania surface.[27] This so-called strong metal-support interaction (SMSI) state generally occurs at high temperature.[28] Experiments were not made under such conditions. Experimental spectra do not reflect any strong metal-support interaction. Therefore, we think that the possibility of a three-oxygen-bound Rh(allyl)(H) complex on ideal hydroxylated TiO_2 (011) surface is unlikely.

Comments

One might ask whether it is possible to compare our theoretical results with experiment. Ultraviolet photoelectron spectroscopy (UPS) data indicate that the presence of the oxide-bound bis(allyl)rhodium complex on the oxide surface is characterized by two new peaks.[2] These are attributed to allyl ligands MO's at lower energy, and to Rh 4d-π_2 allyl MO's at higher energy relatively to the oxygen peak. In addition, the oxygen peak shifts 0.7 eV to lower energy, indicating oxygen-rhodium bonding. The suppression of Ti 3d peak upon tris(allyl)rhodium adsorption, which characterized a reduced hydroxylated TiO_2 surface, is in agreement with our conclusions, i.e. the Ti 't_{2g}' states might constitute a 'reservoir' which can be emptied or filled, depending on the electronic requirements of adsorbates.

The information extracted from the UPS data agrees rather well with our results. Figures 7 and 8 show a slight down shift of rhodium-bound oxygen peak. Occupied Rh-allyl states are "inserted" between titanium t_{2g} and oxygen peaks. Beyond the latter peak, at lower energy, some allyl ligand states are found in resonance with the hydroxyl band.

The oxide-bound Rh(allyl)(H) catalyst produced upon H_2 exposure leads to a diminution of the allyl UPS feature and some changes near the Fermi region. A shift of the O emission to higher energy occurs. We do not see this peak shift in our calculations. In the cases of Rh(allyl)$_2$ and Rh(allyl)(H), the rhodium-bound oxygen peak was centered at ca.-15 eV (see Figures 7 and 9), and the Rh-O overlap populations were rather similar. On the other hand, stronger Rh-C overlap populations were noted in the Rh(allyl)(H) case.

Tris(allyl)rhodium experiments have been also performed on hydroxylated Al_2O_3 surfaces. Despite some slight differences such as sticking probability, thermal decomposition, similar results for the two inorganic supports, hydroxylated Al_2O_3 and TiO_2, were observed.[2b] The electronic structure of ideal hydroxylated alumina surfaces such as α-Al_2O_3 (0001) is expected to be quite different from that of TiO_2.[29] Assuming that hydroxyl groups form the topmost surface layer of an α-Al_2O_3 (0001) face, 22, every Al atom is bulk-like, i.e. surrounded by a

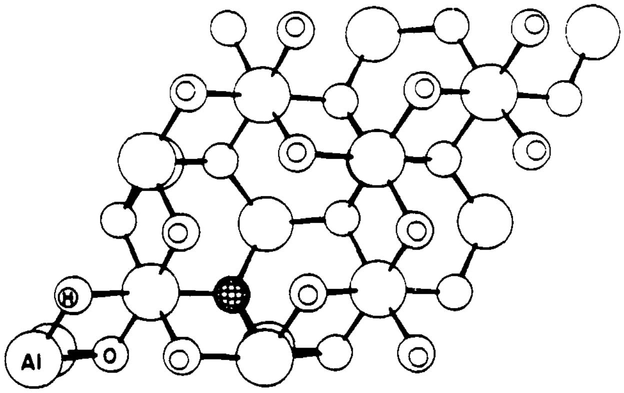

top view

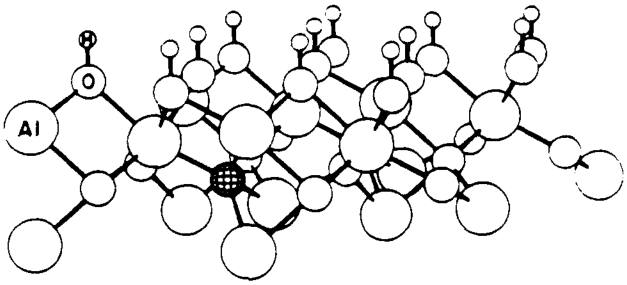

side view

22

distorted oxygen octahedron.[30] Therefore, the DOS of a hydroxylated Al_2O_3 (0001) surface would be comparable to the one obtained for bulk α-Al_2O_3[31] (at least the top of the valence band and the bottom of the conduction band). The DOS of ideal hydroxylated Al_2O_3 (0001) exhibits a very large energy gap separating the top of the valence band from the bottom of the conduction band.[32] No empty or filled states are in resonance with the HOMO/LUMO's of organo-rhodium species. Thus, it would seem that the conclusions drawn from the study on TiO_2 surfaces (vide supra) are thrown into question: the rutile and alumina surfaces have similar reactivity, yet the alumina support does not seem to have the states required to provide an electron reservoir for support-adsorbate electron flow.

Perhaps the problem is in assuming a perfect alumina support. The oxide Al_2O_3 was prepared by exposing aluminum surfaces to water vapor. Interaction of H_2O with aluminum leads to its dissociation and rapid passivation of the aluminum surface.[22b] Studies of H_2O adsorption on an Al(100) surface have shown that Al_2O_3 oxide starts to grow, forming islands and leading to more or less closed Al_2O_3 film.[33] Therefore, oxygen-vacancy point defects must be present in the Al_2O_3 oxide film. Moreover, impurities can also be trapped. To understand the electronic effect of oxygen vacancies, we investigated a defect model corresponding to the removal of one oxygen atom from the sub-surface oxygen layer per unit cell (see shaded O atoms in 22). The O/Ti ratio is reduced from 1.5 in ideal hydroxylated

(0001) surface to 1.44. This corresponds to one O-vacancy for 16 Al atoms. Four bonds have to break to create an O-vacancy. The oxygens are removed as neutral atoms, therefore the four aluminums surrounding every O-vacancy are formally reduced from Al^{3+} to $Al^{2.5+}$. The DOS obtained from calculations on a (2x2) super-cell exhibits a number of peaks in the band gap resulting mainly from the Al atoms surrounding the vacancy.[34] The removal of the O atom allows the four Al atoms to overlap and interact together. The Al...Al contacts are rather short (2.65/3.50Å), therefore their interaction gives some occupied bonding and vacant antibonding states, explaining the different peaks "inserted" in the band gap. These Al atoms are expected to relax because of the empty space between them. Consequently the shape of the DOS will be somewhat modified. Nevertheless, the main feature should remain, i.e. O-vacancy point defects in Al_2O_3 induce new filled/empty Al states capable of resonating with the FMO's of the organo-rhodium adsorbate, thus activating the system.

Conclusions

Two major conclusions can be drawn from our study of the adsorption of organo-rhodium complexes on metal oxide supports. The presence of oxide support states in resonance with FMO's of the organometallic adsorbate may facilitate the activation of the latter. These states can act as a reservoir, now storing now giving up electrons, according to the electronic requirements of the adsorbate. Pouring electron into rhodium-allyl antibonding levels seems to be necessary to activate tris(allyl)rhodium species. Matching of oxide surface states with adsorbate FMO's is an important parameter. For example tris(allyl)rhodium reacts with Al_2O_3 while tetra(allyl)zirconium does not.[2b] The composition and the nature of the inorganic support surface plays also an important role. Different results for adsorption of tris(allyl)rhodium on polycrystalline TiO_2 have been claimed.[35]

Both terminal and bridging modes of anchoring can be encountered for the rhodium(III) center. Immobilization of the rhodium complex occurs primarily via bonding interactions between vacant Rh d orbitals and lone pairs from the support oxygen atom(s).

Acknowledgment. We are grateful to J. Schwartz, S. Bernasek and their groups for stimulating us to approach these problems, and for providing us with much experimental information. J.-F. Halet would like to thank M. Zonnevylle and J. Li for sharing their expertise. His stay at Cornell was made possible by a grant from an Exchange Program between the NSF and the CNRS. We are grateful to J. Jorgensen and E. Fields for the drawings and J. Barrows for the typing of this manuscript. Our work was supported by the Office of Naval Research.

Appendix

Extended Hückel parameters used in both molecular and surface calculations are listed in Table 5.

Table 5 here

In all calculations the following bond distances (Å) were used: Rh-O=2.00; Rh-C=2.15; Rh-H=1.65; O-H=0.96; C-H=1.09. Allyl centroid-Rh-allyl centroid and allyl centroid-Rh-H angles of 170° were assumed.

All surface calculations were of the tight-binding[36] extended Hückel type[37]. Calculations of the hydroxylated TiO_2 (011) surface of symmetry p1 were made using a two-dimensional slab 8.5 Å thick. A TiO_2(011)-p(2x1) system, 3.5 Å thick was taken with organo-rhodium adsorbates. In both cases 9 k-points were used in the irreducible part of the BZ. Calculations on an ideal hydroxylated Al_2O_3 (0001) surface of symmetry p6mm were made assuming a slab 13 Å thick. Calculations on O-vacancy hydroxylated Al_2O_3 (0001)-p(2x2) surface of symmetry p6mm were performed using a slab 4.3 Å thick. 10 and 6 k-points were used respectively. K-point sets were chosen according to the Ramirez and Böhm method.[38]

Table 5. Extended Hückel Parameters.

Orbital		Hii(eV)	ζ_1^a	ζ_2^a
H	1s	-13.60	1.30	
C	2s	-21.40	1.625	
	2p	-11.40	1.625	
O	2s	-32.30	2.275	
	2p	-14.80	2.275	
Al	3s	-12.65	1.550	
	3p	-8.00	1.550	
Ti	4s	-8.97	1.500	
	4p	-5.44	1.500	
	3d	-10.81	4.550(0.4391)	1.60(0.7397)
Rh	5s	-8.09	2.135	
	5p	-4.57	2.100	
	4d	-12.50	4.250(0.5807)	1.97(0.5685)

[a] Exponents and coefficients (in parentheses) in a double zeta expansion of the metal d orbitals.

References

1. (a) Schwartz, J.; Kitajima, N. in "Fundamental Research in Homogeneous Catalysis"; Shilov, A. E., Ed.; Gordon and Breach Science Pub., 1984, Vol. 3, 1003.

   (b) Schwartz, J. Acc. Chem. Res., 1985, 18, 302.

   (c) Iwasawa, Y. in "Catalysis by Metal Complexes: Tailored Metal Catalysts", Iwasawa, Y., Ed.; Reidel, 1986, 1.

   (d) Iwasawa, Y. Adv. Catal., 1987, 35, 187.

   (e) Yermakov, Yu. I.; Kuznetsov, B. N.; Zakharov, V. "Catalysis by Supported Complexes", Elsevier: Amsterdam, 1981.

2. (a) Smith, P. B.; Bernasek, S. L.; Schwartz, J.; McNulty, G. S. J. Amer. Chem. Soc., 1986, 108, 5654.

   (b) Smith, P. B. Ph. D. Thesis, Princeton, 1986.

3. F. F. Wolkenshtein, "The Electronic Theory of Catalysis on Semiconductors", Pergamon Press: Oxford, 1963.

4. (a) Tsukada, M.; Adachi, H.; Satoko, C. Prog. Surf. Sci., 1983, 14, 113.

   (b) Zhidomirov, G. M.; Kazansky, V. B. Adv. Catal., 1986, 34, 131.

   (c) Wolfram, T.; Ellialtioglu, S. in "Theory of Chemisorption", Smith, J. R., Ed.; Springer-Verlag: Berlin, 1980, 149.

5. (a) Cimino, A.; Carra, S. "Studies in Physical and Theoretical Chemistry: Electrodes of Conductive Metallic

Oxides", Trasatti, S., Ed.; Elsevier, 1980, Vol. 11, 97.

6. Wilke, G.; Bogdanovic, B. *Angew. Chem.*, 1961, 73, 756.

7. Henc, B.; Jolly, W.; Salz, R.; Stobbe, S.; Wilke, G.; Benn, R.; Mynott, R.; Seevogel, S.; Goddard, R.; Krüger, C. *J. Organomet. Chem.*, 1980, **191**, 449.

8. Powell, J.; Shaw, B. L. *J. Chem. Soc. Chem. Commun.*, 1966, 236, 323.

9. Pantini, G.; Racanelli, P.; Immirzi, A.; Parri, L. *J. Organomet. Chem.*, 1971, 33, C17.

10. Alcock, N. W.; Conneely, J. A. *Acta Crystallogr.*, 1977, B33, 141.

11. Elian, M.; Hoffmann, R. *Inorg. Chem.*, 1975, **14**, 1058.

12. Hoffmann, R.; Howell, J. M.; Rossi, A. R. *J. Amer. Chem. Soc.*, 1976, **98**, 2484.

13. Rossi, A. R.; Hoffmann, R. *Inorg Chem.*, 1975, **14**, 365.

14. Bönnemann, H. *Angew. Chem. Int. Ed. Engl.*, 1970, 9, 736.

15. For a theoretical study of rutile see:

    (a) Grunes, L. A.; Leapman, R. D.; Wilker, C. N.; Hoffmann, R. *Phys. Rev.*, 1982, **B25**, 7157.

    (b) Burdett, J. K. *Inorg. Chem.*, 1985, **24**, 2244.

16. Cronemeyer, D. C., *Phys. Rev.*, 1952, **87**, 876.

17. Henrich, V. E. *Rep. Prog. Phys.*, 1985, **48**, 1481 and references therein. Ibid *Phys. Chem. Minerals*, 1987, **14**, 396.

18. (a) Tsukada, M.; Adachi, H.; Satoko, C. *Prog. Surf. Sci.*, 1983, **14**, 113.

(b) Munnix, S.; Schmeits, M. Phys. Rev., 1984, B30, 2202.

19. Munnix, S.; Schmeits, M. Phys. Rev., 1985, B31, 3369.

20. (a) Göpel, W.; Anderson, J. A.; Frankel, D.; Jaehnig, M.; Phillips, J.; Schafer, A.; Rocker, G. Surf. Sci., 1984, 139, 333.

(b) Knotek, M. L.; Houston, J. E. Phys. Rev., 1977, B15, 4580.

(c) Bursill, L. A.; Blanchin, M. G. J. Solid State Chem., 1984, 51, 321.

21. Firment, L. E., Surf. Sci., 1982, 116, 205.

22. (a) For a theoretical study see Kawai, T.; Tsukada, M.; Adachi, A.; Satoko, C.; Sakata, T. Surf. Sci., 1979, 81, L640. Tsukada, M.; Shima, N. Phys. Chem. Minerals, 1987, 15, 35.

(b) Thiel, P. A.; Madey, T. E. Surf. Sci. Rep., 1987, 7, 290 and references therein.

(c) Suda, Y.; Morimoto, T. Langmuir, 1987, 3, 786 and references therein.

23. Smith, P. B.; Bernasek, S. L. Surf. Sci., 1987, 188, 241.

24. Hoffmann, R. Angew. Chem. Int. Ed. Engl., 1987, 26, 846.

25. Henrich, V. E.; Kurtz, R. L. Phys. Rev., 1981, B23, 6280.

26. Hoflund, G. B.; Yin, H.-L.; Grogan, A. L., Jr.; Asbury, D. A.; Yoneyama, H.; Ikeda, O.; Tamura, H. Langmuir, 1988, 4, 346.

27. (a) Sakellson, S.; McMillan, M.; Haller, G. L. J. Phys. Chem., 1987, 90, 1733.

(b) Resasco, D. E.; Weber, R. S.; Sakellson, S.; McMillan, M.; Haller, G. L.; J. Phys. Chem., 1988, 92, 189.

(c) Sadeghi, H. R.; Henrich, V. E. J. Catal., 1988, 109, 1.

28. Tauster, S. J. Acc. Chem. Res., 1987, 20, 389 and references therein.

29. Though Al_2O_3 is found in different structural forms such as α- and -Al_2O_3, spectral data indicate their densities of states are rather similar (see Balzarotti, A.; Bianconi, A. Phys. Status Solidi, 1976, B76, 689). We studied the α-alumina (0001) surface.

30. Lewis, J.; Schwarzenbach, D.; Flack, H. D. Acta Crystallogr., 1982, A38, 733.

31. (a) Tossel, J. A. J. Phys. Chem. Solid, 1975, 36, 1273.

(b) Evarestov, R. A.; Ermosthkin, A. N.; Lovchikov, V. A. Phys. Status Solidi, 1980, B99, 387.

(c) Batra, I. P. J. Phys. C: Solid State Phys., 1982, 15, 5399.

(d) Balzarotti, A.; Antonangeli, F.; Girlanda, R.; Martino, G. Phys. Rev., 1984, B29, 590.

(e) Nagel, S. J. Phys. C: Solid State Phys., 1985, 18, 3673.

(f) Causâ, M.; Dovesi, R.; Roetti, C.; Kotomin, E.; Saunders, V. R. Chem. Phys. Lett., 1987, 140, 120.

(g) Pisani, C.; Causâ, M.; Dovesi, R.; Roetti, C. Prog. Surf. Sci., 1987, 25, 119.

32. Bulk α-Al_2O_3 is a very strong insulator. A gap of ca. 9.5eV

has been reported: Arakawa, E. T.; Williams, M. W. *J. Phys. Chem. Solids*, 1968, **29**, 735.

33. Ciraci, S.; Batra, I. P. *Phys. Rev.*, 1983,**B28**, 982.

35. (a) Iwasawa, Y.; Sato, H. *Chem. Lett.*, 1985, 507.

    (b) Asakura, K.; Iwasawa, Y.; Kuroda, H. *J. Chem. Soc. Faraday Trans. 1*, 1988, **84**, 1329.

36. (a) Whangbo, M.-H.; Hoffmann, R. *J. Amer. Chem. Soc.*, 1978, **100**, 6093.

    (b) Whangbo, M.-H.; Hoffmann, R.; Woodward, R. B. *Proc. R. Soc. London Ser. A*, 1979, **366**, 23.

37. Hoffmann, R. *J. Chem. Phys.*, 1963, **39**, 1397.

38. Ramirez, R.; Böhm, M. C. *Int. J. Quant. Chem.*, 1986, **30**, 391.

Figure Captions

Figure 1. Interaction diagram for $[Rh(allyl)_2(OH_2]^-$ (the numbers in parentheses indicate the percentage metal character).

Figure 2. Interaction diagram for $Rh(allyl)_2(OH)$.

Figure 3. Interaction diagram for $Rh(allyl)(H)(OH)$.

Figure 4. Interaction diagram for $[Rh(allyl)(H)(OH)_2]^-$.

Figure 5. Total DOS (dashed line) and the hydroxyl contribution (lined area) of the hydroxylated TiO_2 (011) surface.

Figure 6. Density of states of TiO_2 bulk.

Figure 7. (a) Total DOS (dashed line) and active oxygen contribution (lined area) for hydroxylated TiO_2 (011) support before interaction.

(b) Total DOS (dashed line), active oxygen (lined area) and bis(allyl)Rh (solid line) contributions when bis(allyl)Rh is linked to one oxygen atom from hydroxylated TiO_2 (011) support.

(c) Total DOS for the bis(allyl)Rh layer before interaction. The sticks refer to the MO's of an isolated bis(allyl)Rh fragment.

Figure 8. Total DOS (dashed line), $Rh(allyl)_2$ contribution (solid line) and oxygen contribution (lined area) when $Rh(allyl)_2$ is linked to two oxygen atoms of the hydroxylated TiO_2 support.

Figure 9. (a) Total DOS (dashed line), active oxygen (lined

area) and Rh(allyl)(H) (solid line) contributions when Rh(allyl)(H) is linked to one oxygen atom from the hydroxylated TiO_2 support.

(b) Total DOS for the Rh(allyl)(H) layer before interaction. MO's of an isolated Rh(allyl)(H) group are shown on the far right.

Figure 10. Total DOS (dashed line), active oxygen (lined area) and Rh(allyl)(H) (solid line) contributions when Rh(allyl)(H) is linked to two oxygen atoms from the hydroxylated TiO_2 support.